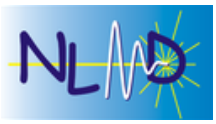

Nonlinear Magnetic Dynamics

Bachelor Thesis

Conservation of Angular Momentum in Magnetic Dynamic Processes

by

Lena Funcke

Supervisor and First Evaluator:	Second Evaluator:	Tutors:
Prof. Dr. Sergej Demokritov	Dr. Vladislav Demidov	Dr. Henning Ulrichs Dr. Oleksandr Dzyapko

A thesis submitted in partial fulfilment of the requirements for the degree of Bachelor of Science in Physics

submitted to the

Faculty of Maths and Natural Sciences

of the

Westfälische Wilhelms-Universität Münster,

prepared at the

Institute of Applied Physics

2nd September 2014

Declaration of Authorship

Hiermit versichere ich, dass die vorliegende Arbeit über "Conservation of Angular Momentum in Magnetic Dynamic Processes" selbstständig verfasst worden ist, dass keine anderen Quellen und Hilfsmittel als die angegebenen benutzt worden sind und dass die Stellen der Arbeit, die anderen Werken – auch elektronischen Medien – dem Wortlaut oder Sinn nach entnommen wurden, auf jeden Fall unter Angabe der Quelle als Entlehnung kenntlich gemacht worden sind.

_____ Münster, 2nd September 2014

[Lena Funcke] [Place, Date]

Ich erkläre mich mit einem Abgleich der Arbeit mit anderen Texten zwecks Auffindung von Übereinstimmungen sowie mit einer zu diesem Zweck vorzunehmenden Speicherung der Arbeit in einer Datenbank einverstanden.

_____ Münster, 2nd September 2014

[Lena Funcke] [Place, Date]

Westfälische Wilhelms-Universität Münster

Abstract

Faculty of Maths and Natural Sciences
Institute of Applied Physics

Bachelor of Science

Conservation of Angular Momentum in Magnetic Dynamic Processes

by Lena Funcke

The current thesis provides a brief overview of several aspects of magnetic dynamic processes, especially the conservation of the angular momentum.
The first issue this thesis considers is whether it is possible to measure experimentally the mechanical oscillations of a magnetic film caused by an elliptic magnetization precession under the condition of the ferromagnetic resonance. This effect is a dynamic analogon of the static effect that was originally discovered by Einstein and de Haas and relies on the total angular momentum conservation of the magnetic subsystem and the lattice. The elliptical precession of the magnetization is associated with an oscillation of the longitudinal component of the magnetization. Therefore, the angular momentum conservation law demands that this oscillation is compensated by a corresponding mechanical oscillation of the sample. In order to determine the amplitude of the mechanical oscillation of the film, an experimental design of this film was simulated in this thesis. However, the simulations indicated that this amplitude is too small for detection by currently available experimental techniques.
In the second train of thoughts, the thesis presents simulations of the three-magnon splitting process, a non-linear process that is caused by the presence of the magnetic dipolar interaction between magnons. Earlier experimental and theoretical findings, related to this splitting, pointed out the incompleteness of the quantum description of the process, if the interaction between the magnetic subsystem and the lattice of the magnetic sample is ignored. Therefore, the three-magnon splitting factor characterizing the increase of angular momentum in the process was determined in this thesis to confirm the existence of some basic theoretical problems in the quantum mechanical description of the magnonic quasi-particles which ignores the lattice.

Acknowledgements

Although I owe a debt of gratitude to various people, only few of them can be considered within this preamble.
To begin with, I would like to express my sincere thanks to Prof. Dr. *Sergej Demokritov* for taking care of my initial enquiry to complete my bachelor's thesis at this institute, for allowing me to join his working group and for cooking me a cuppa tea in a moment of frustration when the work of months turned out to yield no results. Furthermore, the thanks are also due to Dr. *Vladislav Demidov*, who consented to be the second evaluator of my work.
Above all, a heartfelt debt of gratitude is owed to Dr. *Henning Ulrichs* for introducing me into this new field of micromagnetic simulation and dedicating so much time to all of my questions, no matter how inexperienced they sounded. It was an enriching experience to discuss the issues raised within the progress of the thesis with him, and I am thankful that he endured my pigheadedness until both of us were satisfied with the outcomes. Similarly, Dr. *Oleksandr Dzyapko* deserves my specific thanks for introducing me into the experimental work in the beginning of my thesis and for extensively discussing several simulation questions and the physical interpretation of the results with me in the end.
And also the other members of the working group *Nonlinear Magnetic Dynamics* must not be forgotten, since they were the reason why this four months will remain as a pleasant memory. Here, I would like to thank especially *Philipp Seibt*, *Michael Evelt* and *Aleksandr Sadovnikov* for their support whenever I needed help with handling the sometimes inscrutable Linux and for a friendly, funny and warmly atmosphere in the office.
Concerning my whole Bachelor studies I would like to thank all my professors for sharing their knowledge of this highly fascinating subject with me, for their support and their friendly attitude making it a pleasure to study physics at this university. Here, also my fellow students, tutors and the teams of the examination and international offices have to be mentioned and thanked for a pleasant and uncomplicated cooperation.
Last, but far from least, my deepest gratitude is due to my boyfriend, my family and my friends who encouraged me whenever sluggish work and unexpected results raised frustration. Thanks to you all!

Contents

List of Figures

Abbreviations & Symbols

$\boldsymbol{H}$	Static magnetic field
$\boldsymbol{h}$	Dynamic magnetic field
$\boldsymbol{B}$	Static magnetic flux density
M_0	Saturation magnetization
$\boldsymbol{M}$	Magnetization vector
m_i	Dynamic magnetization along dimension i
M_z	Static z component of magnetization
ΔM_z	Maximal reduction of static z component of magnetization
a_k	New variables for magnetization components
α	Gilbert damping constant
$\hbar$	Reduced Planck constant, $\hbar = \frac{h}{2\pi} = 1.05457 \cdot 10^{-34}\text{Js}$
μ_0	Vacuum permeability, $\mu_0 = 4\pi \cdot 10^{-7} \frac{\text{N}}{\text{A}^2}$
t	Time
A	Exchange constant
l_{ex}	Exchange length
N_i	Demagnetization factors along dimension i
λ	Wave length
k	Wave number $k = \frac{2\pi}{\lambda}$, absolute value of wave vector $\boldsymbol{k}$
ϑ_k	Angle between magnetic precession and $\boldsymbol{k}$
m_e	Mass of electron, $m_e = 9,109 \cdot 10^{-31}\text{kg}$
e	Charge of electron, $e = -1.602 \cdot 10^{-19}\text{C}$
g	g-factor of electron, $g = -2.00232$

$\boldsymbol{s}$	Spin of electron
μ_B	Bohr magneton
γ	Gyromagnetic ratio
$\boldsymbol{\mu}_s$	Spin-magnetic moment of electron
f	Frequency
ω	Radial frequency
ω_H	Static field frequency
ω_M	Magnetization frequency
ω_0	Resonance frequency
ω_{r0}	Relaxation frequency
ω_p	Pumping frequency
$P(f)$	Fourier power as a function of frequency f
$E(f)$	Fourier energy = integrated Fourier power as a function of frequency f
l_1, l_2, l_3	Length (x), width (y) and height (z) of YIG film
ρ	Density of YIG film
m	Mass of YIG film
J	Moment of inertia of YIG film
φ	Oscillation angle of YIG film
β	Mechanical damping constant of YIG film
YIG	Yttrium iron garnet, a ferrimagnetic insulator with $\alpha < 10^{-4}$, $A = 3.7 \cdot 10^{-12} \frac{\mathrm{J}}{\mathrm{m}}$, $M_0 = 139260 \frac{\mathrm{A}}{\mathrm{M}}$, $\gamma = 1.7588 \cdot 10^{11} \frac{\mathrm{T}}{\mathrm{s}}$, $\rho = 5.17 \cdot 10^3 \frac{\mathrm{kg}}{\mathrm{m}^3}$.
FMR	Ferromagnetic resonance
LL eq.	Landau-Lifshitz equation
LLG eq.	Landau-Lifshitz-Gilbert equation

"Nature isn't classical, dammit, and if you want to make a simulation of nature, you'd better make it quantum mechanical, and by golly it's a wonderful problem, because it doesn't look so easy."

— R. P. Feynman, *[Fey82, p. 486]*

Chapter 1

Introduction

The research field of magnonics has the intention to explore the quasi-particles magnons. These quantized spin waves are elementary spin excitations in magnetic materials.
During the last years, scientific interest in the field of magnonics as a sub field of spintronics has continuously increased as magnons can garner, transmit and process information. Hence, one can regard spintronics as a new paradigm for prospective information technologies (cf. [WAB+01, p. 1] and [Ulr14, p. 1]); however, the underlying physics has to be further explored before spintronics can actually be used for practical purposes.
First of all, technical disturbances might occur due to macroscopic effects of the magnetization precession on the mechanics of the magnetic sample. Therefore, the interest in an experiment arose with the purpose to determine the amplitude of macroscopic torsional oscillations of a YIG film caused by an elliptic magnetization precession. As former rough estimations indicated an amplitude barely large enough to be measured, the exact characteristics of the film oscillation will be ascertained analytically as well as numerically in this thesis.
Moreover, the thesis presents simulations of the three-magnon splitting process, a non-linear process that is caused by the presence of interaction between magnons. Concerning this splitting, earlier experimental and theoretical findings [KDD+11] pointed out the incompleteness of the quantum description of the related interaction between the magnetic subsystem and the lattice of the magnetic sample. Hence, in this thesis the splitting factor characterizing the increase of angular momentum in the three-magnon splitting process is ascertained to confirm the existence of some basic theoretical problems in the quantum mechanical description of the magnonic quasi-particles, which ignores the lattice dynamics.

In general, all these presented issues are related to the conservation of angular momentum in the magnetic system which is the main topic of this thesis. It is structured as follows:

Chapter 2 presents an introduction into the theory of magnetic dynamic processes in a magnetic film. Fundamental properties of magnetic systems will be introduced, followed by an overview of different types of magnetic oscillations. Firstly, uniform precession of magnetization is explained, and, secondly, a qualitative and mathematical description of spin waves and splitting processes is elucidated. In preparation for the subsequent chapter, the time-dependent change of the magnetization component of the elliptic magnetization precession, that is parallel to the field, is derived. This is required for further calculations describing the Einstein de Haas effect presented in

Chapter 3 which starts with a short historical overview on the Einstein de Haas experiment showing that the angular momentum of a magnetic subsystem is coupled to the one of the lattice. Afterwards, an adjusted experimental design is presented that considers the oscillation of a magnetic cuboid induced by the elliptic magnetization precession. Subsequently, the mathematical background of the related quantum mechanical entities gyromagnetic ratio and Landé factor is given. Moreover, the macroscopic torsional oscillations of the cuboid caused by the elliptic magnetization precession are described.

Chapter 4 presents the programs used for the simulations, the optimal simulation parameters and the evaluation methods of the obtained numerical data. Furthermore, the different approaches to the two simulation topics are explained, leading to the results displayed in

Chapter 5 which comprises the results as well as their discussion. Initially, the analytically and numerically determined oscillation amplitudes of the magnetic cuboid are compared. Subsequently, the splitting factor in three-magnon splitting and the consequent spin and magnetic moment of the magnons are ascertained.

Chapter 6 consists of a short conclusion and emphasizes the huge impact the clarification of the mentioned inconsistencies would have on this field of research.

Finally, in the appendices A, B, C and D one finds theoretical derivations clarifying some statements presented in the theoretical chapters. The last appendix E contains commented scripts and further data illustrating the process and the results of this thesis.

Chapter 2

Theory of Dynamic Processes in a Magnetic Film

2.1 Fundamental Considerations

The following theoretical considerations of this chapter, including the formulas as well as the connections, are mainly taken from [GM96] and partly also from [NB14] and [Ulr14].
The collective magnetism in a ferromagnetic material is caused by the exchange interaction of the electrons leading to an unbalanced spin system. The resulting net spins align spontaneously for temperatures below the Curie point [Kit53, pp. 356f.].
Herring and Kittel [HK51, p. 5] introduced the magnetization $\boldsymbol{M}$, a continuously differentiable vector field, to replace the individual spins $\boldsymbol{s}$ as measures describing the system. This micromagnetic approach describes the magnetization as a macroscopical entity

$$\boldsymbol{M} = \frac{1}{V} \sum_i \boldsymbol{\mu}_{\boldsymbol{s}_i} \tag{2.1}$$

constituted microscopically by the spin-magnetic moments

$$\boldsymbol{\mu}_{\boldsymbol{s}_i} = -g\mu_B \boldsymbol{s}_i, \tag{2.2}$$

where V is the volume of the magnetic sample, g is the Landé factor of an electron and $\mu_B = \frac{e\hbar}{2m_e}$ is the Bohr magneton with $\hbar$ as the reduced Planck constant, e as the charge and m_e as the mass of an electron. When applying an external magnetic field $\boldsymbol{H}$, the spins start to align along the field. Above a certain field strength, all spins point in the direction of the field and the saturation magnetization $\boldsymbol{M}_0$ is reached.

If one wants to consider the dynamics of a magnetic system, the fundamental equation describing the precession of magnetization in a solid body is the following non-linear equation of motion,

$$\frac{\partial \boldsymbol{M}}{\partial t} = -\gamma \boldsymbol{M} \times \boldsymbol{H}_{eff}, \tag{2.3}$$

known as the Landau-Lifshitz (LL) equation (cf. [LP92, p. 278]) with $\gamma = \frac{g\mu_B}{\hbar}$ and the effective magnetic field

$$\boldsymbol{H}_{eff} = \boldsymbol{H}_0 + \boldsymbol{H}_{ex} + \boldsymbol{h} + \boldsymbol{h}_M. \tag{2.4}$$

$\boldsymbol{H}_0$ combines the static external and demagnetizing field, $\boldsymbol{H}_{ex}$ the effective field of the exchange interaction, $\boldsymbol{h}$ represents the alternating component of the external field and $\boldsymbol{h}_M$ is the alternating demagnetizing field.
For a system with damping, the Landau-Lifshitz-Gilbert (LLG) equation has to be used (cf. [Sat11, p. 26]),

$$\frac{\partial \boldsymbol{M}}{\partial t} = -\gamma \boldsymbol{M} \times \boldsymbol{H}_{eff} + \frac{\alpha}{M_0} \boldsymbol{M} \times \dot{\boldsymbol{M}}, \tag{2.5}$$

which contains the Gilbert damping term and will be important in the following section.

2.2 Uniform Precession

In a magnetic system with $\boldsymbol{M} \parallel \boldsymbol{H} \parallel \boldsymbol{e}_z$, an external stimulus can deflect the magnetization from its static equilibrium position so that it starts to precess around $\boldsymbol{H}$ as stated by the LL eq. (2.3). If the resulting macroscopic magnetization (cf. fig. 2.1(b)) precesses in phase in different points of the sample (cf. fig. 2.1(a)), this is called a uniform precession.
For an ellipsoidal sample, magnetized along one of its axes, the frequency of this precession is described by the Kittel formula [Kit48, p. 155]

$$\omega_0 = \gamma \sqrt{[H + (N_x - N_z)M_0][H + (N_y - N_z)M_0]}, \tag{2.6}$$

where N_i are the demagnetization factors. For a sample geometry of an infinite film, i.e. $N_x = N_z = 0$ and $N_y = \mu_0 = 4\pi \cdot 10^{-7}$, where the y-axis is perpendicular to the film-plane, while the x- and the z-axis are in the plane, the equation is simplified to

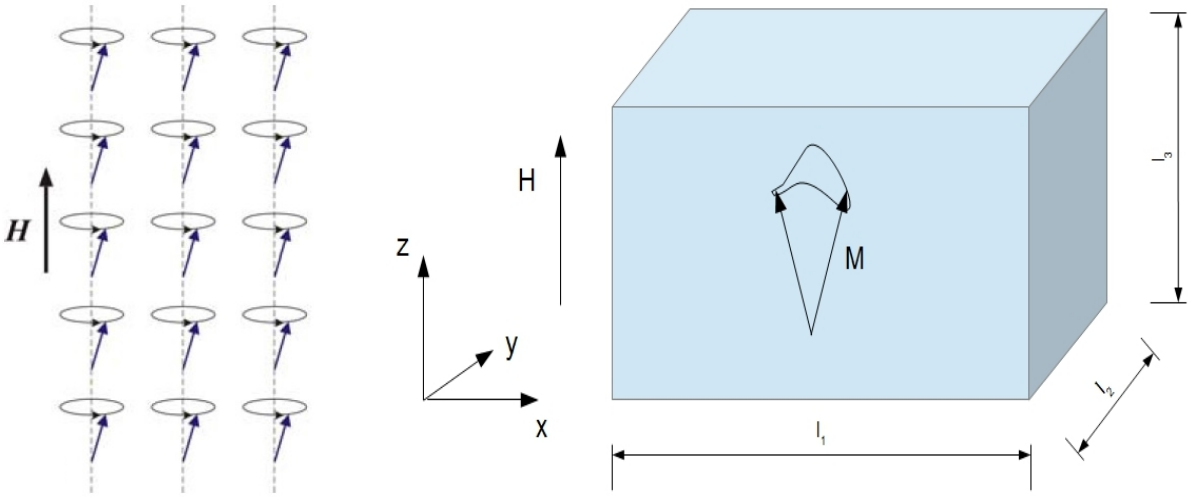

(a) (b)

Fig. 2.1 Schematic figures of (a) a microscopic circular uniform precession of the magnetic moments (figure taken from [Dzy10, p. 14]) and (b) macroscopic elliptic precession of the magnetization in a YIG film.

$$\omega_0 = \gamma\sqrt{H(H + \mu_0 M_0)}. \tag{2.7}$$

In an infinite medium, the uniform precession can be assumed to be circular (cf. fig. 2.1(a)). However, in a tangentially magnetized film with $l_2 << l_1, l_3$, the dynamic dipolar fields induce an ellipticity of magnetic precession (cf. fig. 2.1(b)). When the precessing magnetization vector points out-of-plane, the induced magnetic charges at the opposing surface create a strong demagnetizing field and the vector is pushed back in the direction parallel to the static field $\boldsymbol{H}$. This ellipticity is described mathematically in sec. 2.4.

2.3 Spin Waves

The already described uniform precession of magnetization around the external field can be assumed as a wave with a wave vector of $\boldsymbol{k} = 0$. In general, all wave-like excitations of the equilibrium state of magnetization are called spin waves. However, the spin waves described in this chapter are the propagating ones, having $\boldsymbol{k} \neq 0$ and consisting of magnetic moments that do not precess in phase (cf. fig. 2.2). As the spin waves are collective excitations analogous to lattice vibrations, they can be quantized to quasi-particles, called magnons.
The concept of spin waves was introduced by Bloch [Blo30, p. 4], who derived the dispersion law of spin waves in 1930, but only took into account the exchange interaction. Holstein and Primakoff [HP40, p. 4] included dipolar interaction into their later, more exact theory.

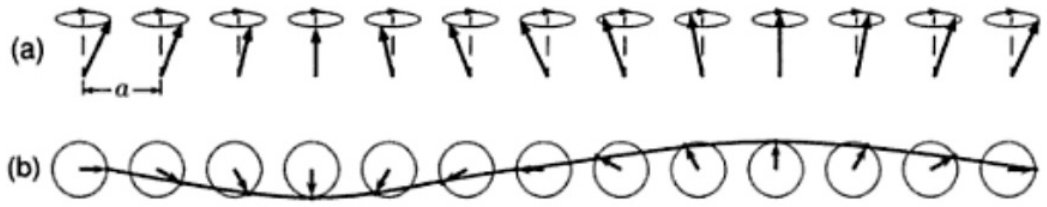

Fig. 2.2 Spin wave in a chain of spins at a distance of a, (a) perspective and (b) top view. One wavelength is shown, the wave line goes through the top of the spin vectors. (figure taken from [Kit53, p. 365])

An approximate dispersion relation of the spin waves in a system with both exchange and the magnetic dipolar interaction was determined by Kalinikos and Slavin (cf. [GM96, p. 181], [KS86, p. 6,7,10,55,60], [Kal80, p.5,6,9]) to

$$\omega^2 = \left(\omega_H + l_{ex}^2 \omega_M k^2\right)\left(\omega_H + l_{ex}^2 \omega_M k^2 + \omega_M \sin^2 \vartheta_k\right), \tag{2.8}$$

where ϑ_k is the angle between $\mathbf{M}$ and $\mathbf{k}$, the frequencies are defined as $\omega_H = \gamma H$ and $\omega_M = \gamma \mu_0 M_0$, and $l_{ex} = \sqrt{\frac{A}{2\pi M_0^2}}$ is the exchange length with A as the exchange constant.

2.3.1 Non-Linear Coupling of Magnetic Modes

One excitation mechanism for spin-waves is the parametric pumping process where several modes with the same frequency but different wave vectors and propagation directions are excited. As described in oscillator theory (cf. e.g. [NM07, p. 15]), a parametrically excited system contains a time-dependent parameter like the magnetic field. Hence, the energy is pumped into the system by a modulation of the internal parameter, in the present case the magnetization. This modulation is achieved by applying a dynamic field $\boldsymbol{h}(t)$, which is perpendicular to the static field $\boldsymbol{H}$.
The perpendicular pumping process is based on non-linear coupling between different spin wave modes. For a mathematical description, one has to assume an approximative form of the magnetization [GM96, p. 247]

$$\boldsymbol{M} = M_0 \boldsymbol{e}_z + \boldsymbol{m}(\boldsymbol{r}, t), \qquad \text{where} \qquad \boldsymbol{m}(\boldsymbol{r}, t) = \sum_{\boldsymbol{k}} \boldsymbol{m}_{\boldsymbol{k}}(t) e^{-i\boldsymbol{k}\boldsymbol{r}} \tag{2.9}$$

is the fourier transformed representation of the dynamic component of the magnetization. After substituting this ansatz into the LL equation (eq. 2.3), one receives two differential equations [GM96, p. 248]

$$-i\frac{da_0}{dt} = \omega_0 a_0 - \gamma(h_x + ih_y) + \Omega_{n0}, \tag{2.10}$$

$$-i\frac{da_k}{dt} = (A_k + \gamma h_z)a_k + B_k a^*_{-k} + \Omega_{nk}. \tag{2.11}$$

The variables and parameters are (cf. [GM96, pp. 247,181] and [Ulr14, p. 7])

$$a_k = \frac{1}{M_0}(m_{\boldsymbol{k}x} + im_{\boldsymbol{k}y}), \quad a^*_{-k} \text{ analogously}, \tag{2.12}$$

$$A_k = \omega_H + l^2_{ex}\omega_M k^2 - \frac{1}{2}\omega_M(P_0(1 - \sin^2\vartheta_k) - 1), \tag{2.13}$$

$$|B_k| = \frac{1}{2}\omega_M(P_0(1 + \sin^2\vartheta_k) - 1). \tag{2.14}$$

$P_0 = \frac{1-e^{-kl_2}}{kl_2}$ is a term which takes into account the finite size of the film in the y direction (constant taken from [GM96, p. 248] and [Ulr14, pp. 6,7]). The expressions Ω_{n0} and Ω_{nk} comprise higher order mixed terms in a_k, a^*_k including a_0 [GM96, p. 248]. Therefore, they describe the interactions between different modes.

2.3.2 Three-Magnon Splitting

In a linear approximation, equation 2.11 and the adjoint equation describe the coupled oscillations of two harmonic oscillators a_k and a^*_{-k}, which correspond to spin waves with wave vectors $\boldsymbol{k}$ and $-\boldsymbol{k}$. The mathematical derivation of this solution can e.g. be found in [ABP68]. However, in a parametric pumping process the uniform mode a_0 is so strongly excited that one has to include also non-linear terms describing the coupling of the uniform mode to other spin wave modes due to Ω_{n0} and Ω_{nk} (cf. [NB14, p. 17]). This energy transfer from the modulating source to the oscillators is most effective if [GM96, p. 250]

$$n\omega_p = \omega_1 + \omega_2 \tag{2.15}$$

with $n = 1, 2, 3, ...$ The frequencies ω_1 and ω_2 are the ones of the spin waves and ω_p is the pumping frequency that modulates the coupling.
Returning to the description of spin waves as quasi-particles, relation 2.15 describes the process of annihilation of n particles with the frequency ω_p and creation of two particles with the frequencies ω_1 and ω_2. At a certain threshold amplitude of the periodic field $\boldsymbol{h}$, the energy transferred to the spin waves exceeds the energy loss that they face, i.e. their

amplitudes start to increase exponentially which results in unstable behaviour. Since the value of n in eq. 2.15 is the order of the instability, the first-order instability corresponds to a three-magnon splitting process. This process is shown in fig. 2.3, where the upper and lower borders of the area indicating the allowed frequencies and wave vectors of the spin waves refer to spin waves propagating perpendicular (Damon Eshbach modes) and parallel (backward volume modes) to the applied field, as labelled. Here, the created magnons (spin waves) with wave vectors $\boldsymbol{k}$ and $-\boldsymbol{k}$ have degenerated energies ($\omega_1 = \omega_2$) to ensure momentum and energy conservation (all these considerations were taken from [GM96, p. 250] and [KDD+11, p. 663]).

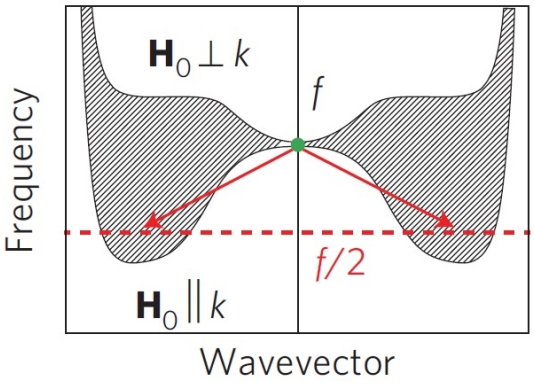

Fig. 2.3 Spin-wave spectrum with indicated three-magnon splitting in YIG (figure taken from [KDD+11, p. 663]).

As explained in [KDD+11, p. 663], the angular momentum, however, is not conserved due to the the increase of the total number of magnons which, according to Bloch's exchange theory, carry an angular momentum equal to $\hbar$ (ref. [Blo30]). Hence, three-magnon splitting is not allowed if an isolated magnetic system is considered, as it was done in Bloch's model only describing the exchange interaction [Blo30]. If one includes the magnetic dipolar interaction, this restriction is removed. Mathematically spoken, the Hamiltonian operator describing the dipolar interaction does not commute with the operator of the angular momentum of the magnetic subsystem alone, but with the operator of the total angular momentum combining the magnetic subsystem and the lattice (cf. [KDD+11, p. 663] and [BSPA59]). Therefore, the quantization of spin waves leading to a spin of 1 is only valid for the total system of magnetic subsystem and lattice.

Therefore, when incorporating the dipolar interaction into the model, the splitting factor characterizing the increase of angular momentum parallel to the static field differs from 2 as parts of the spin are carried by the lattice (cf. e.g. [NB14, pp. 22-26]). Due to this coupling of the magnetic subsystem with the lattice, not the classical magnon but rather a mixture of magnetic and lattice oscillation is an exact eigen excitation of the system. However, as an approximate quantization is used, which provides only the magnetic part of this composite particle, the splitting factor differs from 2. This factor providing information on the magnetic part of both the spin and the magnetic moment of the magnons will be derived numerically in this thesis for specific parameters.

Surprisingly, a coherent quantum treatment of the angular momentum flow from the magnetic subsystem into the lattice and vice versa is still missing, though exchange and dipolar interactions occurring in a ferromagnet have firstly been described quantum mechanically already more than 70 years ago ([KDD+11, p. 663], [HP40], [Maj07]).

2.4 M_z Magnetization Change of Elliptic Precession

The conservation of the angular momentum in the magnetic subsystem that is parallel to the static field is violated not only in the three-magnon process, but also in the elliptic precession of magnetization. This observation will be important in the next chapter where the consequences of the time-dependent change of M_z parallel to $\boldsymbol{H}$ on the magnetic sample are illustrated. In order to calculate this magnetization change, one has to consider weak dynamic fields that cause small dynamic amplitudes $\left|\frac{m_{x,y}}{M_0}\right| << 1$. The magnitude of the magnetization vector $|\boldsymbol{M}|$ has to stay constant due to the conservation of the total magnetic moment. An informative expression for M_z can be derived using basic trigonometry and an expansion for small amplitudes (cf. app. C)

$$M_z = \sqrt{M_0^2 - m_x^2 \cos^2 \omega_p t - m_y^2 \sin^2 \omega_p t} \tag{2.16}$$

$$\approx M_0 - \frac{1}{4M_0}(m_x^2 + m_y^2) + \frac{1}{4M_0}(m_y^2 - m_x^2)\cos 2\omega_p t. \tag{2.17}$$

This equation shows some consequences of the excitation of magnetic precession, which are also illustrated numerically in ch. 4. The second term on the right hand side of the equation describes the reduction of the static component $M_{z,eff} = M_0 - \frac{1}{4M_0}(m_x^2 + m_y^2)$ (effective magnetization), leading to a negative non-linear frequency shift of the dispersion relation 2.8 (cf. [Ulr14, p. 17]). The third term shows that the resulting oscillation of the magnetization with frequency $2\omega_p$ only exists for elliptic and vanishes for circular precession. If eq. 2.17 is rearranged and differentiated with respect to t, one obtains the final expression of the time-dependent change of M_z,

$$\dot{M}_z = 2\omega_p \frac{m_x^2}{4M_0}\left(1 - \frac{m_y^2}{m_x^2}\right)\sin 2\omega_p t \stackrel{!}{=} 2\omega_p \Delta m \cdot \sin 2\omega_p t. \tag{2.18}$$

To describe the strength of the ellipticity of uniform precession, one has to take a look at the ratio of the dynamic magnetization components $m_{x,y}$ perpendicular to the static field[1]

$$\frac{m_y}{m_x} = -i\left(\frac{H + (N_y - N_z)\cdot M_0}{H + (N_x - N_z)\cdot M_0}\right)^{-\frac{1}{2}}. \tag{2.19}$$

This formula is only valid for $\alpha = 0$ and a small initial magnetization deflection. It illustrates that for large static fields the Zeeman energy is much higher than the demagnetization energy

[1] This formula is taken from [GM96, p. 26] apart from the typing error of leaving out the saturation magnetization M_0 which was done in this source.

and the ellipticity vanishes.
Eq. 2.19 equals the ellipticity relation for spin waves,[2]

$$\frac{m_y}{m_x} = -i\left(1 + \frac{\omega_M \sin^2\vartheta_k}{\omega_H + l_{ex}^2\omega_M k^2}\right)^{-\frac{1}{2}} = -i\left(\frac{A_k + |B_k|}{A_k - |B_k|}\right)^{-\frac{1}{2}} \tag{2.20}$$

for $k \to 0$. As it can be easily seen in eq. 2.20, the ellipticity is strongest for uniform precession, i.e. for small wave numbers k with B_k comparable to A_k. For large k, the exchange effect dominates, so that $A_k >> B_k$, and the magnetic precession becomes circular (cf. [Ulr14, p. 16]).
To find a complete expression describing the time-dependent change of M_z, the formula 2.18 raises the need for a term characterizing the component m_x. For this purpose, one has to calculate the amplitude of uniform precession (cf. [Suh57, p. 1,17,22] and [NB14, p. 17]). If one includes spin waves losses via the substitution $\omega_0 \to \omega_0 + i\omega_{r0}$, where ω_{r0} is proportional to the Gilbert constant α, and assumes a circularly polarized dynamic field that oscillates with the pumping frequency w_p, the expression [GM96, p. 249]

$$a_0 = \frac{\gamma h}{\omega_0 - \omega_p + i\omega_{r0}} \cdot e^{i\omega_p t} \tag{2.21}$$

for the amplitude of uniform precession follows, which is twice as large as the precession amplitude when regarding a linear polarized field. When taking into account eq. 2.12 and 2.21, the expression for m_x

$$m_x = \left(1 + i\frac{m_y}{m_x}\right)^{-1} M_0 a_0 = \left(1 + i\frac{m_y}{m_x}\right)^{-1} \frac{M_0\gamma h}{\omega_0 - \omega_p + i\omega_{r0}} \cdot e^{i\omega_p t} \tag{2.22}$$

is obtained. If resonant excitation with $\omega_0 = \omega_p$ is assumed, one can write the real part of m_x as

$$Re(m_x) = \left(1 + \left(\frac{m_y}{m_x}\right)^2\right)^{-1} \frac{M_0\gamma h}{\omega_{r0}} \cdot \cos\omega_p t \tag{2.23}$$

and one receives the same time dependency as already assumed in eq. 2.16.
As mentioned, a complete expression for the time-dependent change of M_z has to derived in order to describe mechanical film oscillations described in the next chapter. For this purpose, one has to insert eq. 2.19 and 2.23 into eq. 2.18.

[2] In [GM96, p. 184], the formula (7.23) referring to eq. 2.20 contains the typing error of leaving out the exterior power of the fraction, which is shown in the app. C.

Chapter 3

Theory of Einstein de Haas Effect

3.1 Historical Overview

In the year 1915, long before the discovery of quantum mechanics, A. Einstein and W. J. de Haas conducted a simple experiment to prove the coupling between the angular momentum and the magnetic moment of single atoms ([EdH15]).

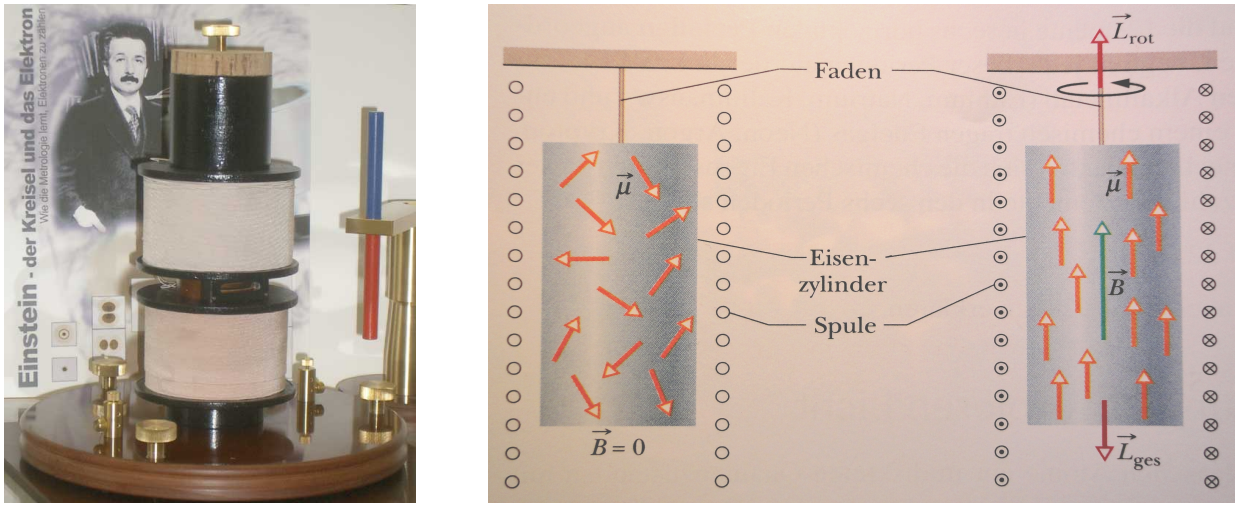

(a) (b)

Fig. 3.1 (a) Replica of the original setup of the Einstein de Haas experiment (figure taken from [DPG]). (b) Schematic setup of the Einstein de Haas experiment. Left side: Without a magnetic field, the magnetic dipole moments $\boldsymbol{\mu}$ point in different, random directions. Right side: When a magnetic field $\boldsymbol{B}$ is applied, The magnetic moments align parallel to the applied external field; their total angular momentum $\boldsymbol{L}_{ges}$ induces a mechanical angular momentum $\boldsymbol{L}_{rot}$.(figure taken from [HRW03, p. 1240])

Einstein and de Haas attached an iron cylinder to a thin string and inserted it into a coil as shown in fig. 3.1(b). In the beginning, the magnetic dipole moments of the atoms in the cylinder pointed in various directions, so that the angular momenta cancel each other out (cf. 3.1(b), left). Subsequently, the coil applied a magnetic field parallel to the cylinder and the magnetic moments aligned parallel to it (cf. 3.1(b), right).
As there were no external torques acting on the cylinder, the total angular momentum remains zero. Hence, if the atomic angular momenta align antiparallel to the magnetic field, they have to transfer an angular momentum to the cylinder, thereby rotating it. Afterwards, the torsion of the string induces a torque stopping the rotation of the cylinder and transposing it into a harmonic torsional oscillation.
This experiment indicated that the mechanical angular momentum and the magnetic moment of an atom are coupled in opposing directions [HRW03, p. 1240]. Furthermore, the resulting relation of the magnetic moment to the angular momentum for the spin was twice as large as for the orbital angular momentum [Dem96, p. 161].
A general conclusion of this experiment is that a change of the angular momentum of a *magnetic* state can cause a *visible* rotation of a macroscopic object.

3.2 Adjusted Experimental Design

To connect the considerations of sec. 2.4 with the static Einstein de Haas effect, macroscopic torsional oscillations of a magnetic film are considered, which are induced by its elliptic magnetization precession.

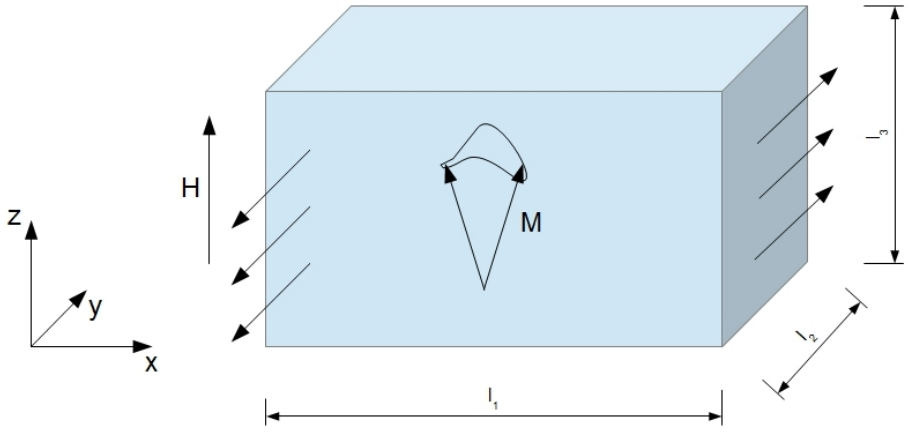

Fig. 3.2 A schematic figure of the elliptic magnetization inducing oscillations of the YIG film.

As mentioned, former estimations indicated that the amplitude of this precession can be barely large enough to be measured. To encourage or reject the possibility to measure this

precession in a real experiment, an adjusted experimental design has to be conducted that will be examined analytically and numerically in the subsequent chapter.
Instead of an iron cylinder, the design consists of a YIG film with a volume of (100·10·100)μm (cf. fig. 3.2). Moreover, the physical principles behind the oscillations examined in this thesis differ slightly from the ones in the original Einstein de Haas experiment. There, angular momentum flew from the magnetic subsystem into the lattice as the spins changed their direction. This situation is comparable to the three-magnon splitting process where the magnetic system is fundamentally excited, so one spin of the system flips and a magnon is created. The resulting rotation of the lattice caused by the angular momentum flow from the lattice into the magnetic subsystem is damped rapidly in case of a single three-magnon splitting process and therefore cannot be observed.
The analytical and numerical calculations in this thesis, however, describe film oscillations induced by the *elliptic precession* of magnetization. Here, the spin part of the angular momentum L_z is not constant, so for a total angular momentum conservation of the whole system, the film has to oscillate mechanically around the z axis. This effect differs from the one in the original static experiment as one now describes a forced oscillation based on a time-dependent, periodical torque acting on the lattice.

3.3 Gyromagnetic Ratio and Landé Factor

The connections of the following theoretical considerations are mainly taken from [Sch].
In order to derive the maximal torque D_{max} acting on the film as induced by the change of the magnetization component parallel to the magnetic field $\dot{M}_z$, one primarily has to consider the gyromagnetic ratio and the Landé factor for the spin of an electron [Dem96, p. 161],

$$\gamma = \frac{\boldsymbol{\mu}_s}{\boldsymbol{s}} = \frac{-ge}{2m_e} \qquad \text{and} \qquad g = \frac{2m_e}{-e}\frac{\boldsymbol{\mu}_s}{\boldsymbol{s}}, \qquad \text{respectively.} \tag{3.1}$$

The whole magnetic moment of the film is $\boldsymbol{\mu}_{film} = N\boldsymbol{\mu}_s$, where $\boldsymbol{\mu}_s$ is the spin-magnetic moment of an electron and N is the number of electrons with an uncompensated spin. Therefore, the magnetization is

$$\boldsymbol{M} = \frac{\boldsymbol{\mu}_{film}}{V} = \frac{N\boldsymbol{\mu}_s}{V}, \tag{3.2}$$

where $V = l_1 l_2 l_3$ is the volume of the film.
The whole magnetic angular momentum of the film is $\boldsymbol{L}_{mag} = N\boldsymbol{s}$, where $\boldsymbol{s}$ is the spin of one electron. From these considerations it follows that

$$g = \frac{2m_e}{-e}\frac{MV}{L_{mag}}. \tag{3.3}$$

Due to the oscillation of the film, the magnetization and the angular momentum of the film are time dependent. As these quantities are the only time-dependent ones in the formula, one can derive them with respect to t and define $D(t) = \dot{L}(t)$,

$$g = \frac{2m_e}{-e}\frac{\dot{M}V}{D_{mag}}. \tag{3.4}$$

In this thesis, only the magnetization change $\dot{M}_z$ is considered, $\dot{M} \triangleq \dot{M}_z$, and one receives the torque acting on the film

$$D_{mag} = \dot{L}_{mag} = \frac{2m_e}{-e}\frac{V\dot{M}_z}{g} = \frac{V\dot{M}_z}{\gamma}. \tag{3.5}$$

At this point, the oscillation amplitude could be derived by considering the conservation of angular momentum: $\dot{\boldsymbol{L}}_{mag} + \dot{\boldsymbol{L}}_{mech} = 0$ (cf. app. A). However, another approach leading to the same result is presented in the following chapter.

3.4 Torsional Oscillations

If one considers a periodic force $F_0 \cdot \cos(2\omega_p t)$ that acts on a mass m attached to a spring with spring constant κ, the equation of motion, [Dem94, pp. 363f.]

$$m\ddot{x} = -\kappa x - b\dot{x} + F_0 \cos(2\omega_p t), \tag{3.6}$$

follows, where x is the free coordinate of the system, $2\omega_p$ as the pumping frequency and b describing the damping of the oscillation. This equation of motion can be converted into the inhomogeneous differential equation

$$\ddot{x} + 2\beta\dot{x} + \omega_0^2 x = K \cdot \cos(2w_p t) \tag{3.7}$$

using the abbreviations

$$\omega_0^2 = \frac{\kappa}{m}, \quad \beta = \frac{b}{2m}, \quad K = \frac{F_0}{m}, \tag{3.8}$$

where ω_0 is the eigen frequency of the undamped oscillation.

To return to the initial adjusted experimental design and aiming for a description of the forced rotary oscillations of the YIG cuboid, one has to consider a torsional oscillation and substitute the Cartesian deflection coordinate x by the oscillation angle φ in eq. 3.7. Furthermore, K can be expressed by

$$K = \frac{F_0}{m} = \frac{D_{max}}{J}, \tag{3.9}$$

where $D = J\frac{d^2\varphi}{dt^2} = J\frac{F}{m}$ [Dem94, p. 150]. D_{max} is the maximal torque exerting the periodical force on the film which possesses the inertial torque J [Dem94, p. 149]

$$J = \frac{1}{12}m(l_1^2 + l_2^2), \tag{3.10}$$

where l_1 is the length (in x direction) and l_2 is the width (in y direction) of the film. The maximal torque therefore amounts to

$$D_{max} = \varphi_0 J\sqrt{(\omega_0^2 - 4\omega_p^2)^2 + (4\beta\omega_p)^2}. \tag{3.11}$$

Thus, one receives a maximal oscillation angle of [Dem94, pp. 365]

$$\varphi_0 = \frac{D_{max}}{J}\frac{1}{\sqrt{(\omega_0^2 - 4\omega_p^2)^2 + (4\beta\omega_p)^2}} \approx \frac{D_{max}}{4J\omega_p^2} \tag{3.12}$$

whereas the approximation neglects both the mechanical damping β and the eigen frequency ω_0, which are small in comparison to the pumping frequency $\omega_p \approx 10^{10}$Hz. To finally obtain the oscillation amplitude of the YIG film in y direction, simple trigonometric considerations and the approximation $\sin(x) \approx x$ for small x lead to

$$y_0 = \frac{l_1}{2} \cdot \sin\varphi_0 \approx \frac{l_1}{2} \cdot \left(\frac{D_{max}}{4J\omega_p^2}\right). \tag{3.13}$$

Subsequently, one can insert eq. 3.5 and 2.18 into the expression 3.13:

$$y_0 = \frac{l_1}{2} \cdot \left(\frac{\dot{M}_{z,max}V}{\gamma} \cdot \frac{1}{4J\omega_p^2}\right) = \frac{l_1}{2} \cdot \left(\frac{2\omega_p\Delta mV}{\gamma} \cdot \frac{1}{4J\omega_p^2}\right) = \frac{l_1}{2} \cdot \left(\frac{\Delta mV}{2J\omega_p\gamma}\right). \tag{3.14}$$

The numerical methods for the determination of a specific value for this amplitude is presented in the subsequent chapter and the result is shown afterwards in ch. 5.

Chapter 4

Simulations

4.1 Programs

All the simulations that will be presented in this thesis were implemented with the micromagnetic simulation program mumax[3], which is GPU-accelerated (cf. [Van]). The simulations comprised a magnetic sample that was segmented in finite, cube-shaped cells. The applied uniform magnetization followed the LL equation (eq. 2.3) in each cell, taking into account i.a. the magnetostatic, exchange and anisotropy interactions. A more thorough explanation can be found in [VVdW].
The display of the similar program OOMMF (Object Oriented MicroMagnetic Framework, cf. [Nat]) was used to review the created magnetic fields and the received magnetization distribution of the simulated cuboid. Statistical analysis was performed using Scilab, Matlab, QtiPlot and Origin.
An exemplary selection of the used codes is presented in the appendix E to gain a deeper insight into the methods of this thesis.

4.2 Simulation Parameters

4.2.1 Micromagnetic Sample

With mumax, a micromagnetic grid with a size of (256, 32, 256) cells was created. The cell sizes were (0.15, 0.16, 0.15)μm so that the whole cuboid had a size of (38.4, 5.12, 38.4)μm. Here, the y size of the cuboid was chosen to 5.12μm as in former experiments [KDD+11] this width was chosen to 5.1μm. The spin waves were described by a wave number of $k = 5.236\frac{1}{\mu\text{m}}$, i.e. a wavelength of $\lambda = 2\pi/k \approx 1.2\mu$m, so the film has to be more extended

than this wavelength to observe the spin waves. Due to long simulation times, the size of the cuboid remained constant so that the optimal values of the other simulation parameters had to be ascertained just once.
As disturbing edge effects obstructed the effective excitation of uniform precession and spin waves, periodic boundary conditions as well as a removal of surface charges were simulated. However, these methods did not result in the desired enhancement of excitation. The implemented alternative solution of this problem was a relatively small cell size and large grid size in y direction, so only the layer y=16 in the homogeneous middle of the cuboid was used to analyse the magnetization distribution of the different excited modes. One negative consequence of the small cell size in y direction were the only 7.5 times larger cuboid sizes in z and x direction, since the cell had to be nearly a cube for effective simulations.

4.2.2 Optimal Static Field $\boldsymbol{H}$

The static magnetic field $\boldsymbol{H}$ was applied in z direction. To gain the optimal field and pumping frequency $f = f_{FMR}$, it was necessary to take into account the dispersion curve of backward volume modes with $\boldsymbol{k} \parallel \boldsymbol{H}$ (cf. fig. 2.3). The excitation was optimal when the secondary magnon frequency $f/2$ was situated directly on the dispersion curve, which means that no further, non-backward volume modes were excited with $\boldsymbol{k} \perp \boldsymbol{H}$. Hence, one had to minimize the dispersion relation (eq. 2.8) to receive the optimal minimal magnon frequency f_{min} for which the three-magnon process was still allowed. Due to $f = f_{FMR} \stackrel{!}{=} 2 \cdot f_{min}$, $\Delta f = f_{FMR} - 2 \cdot f_{min} = 0$ had to be determined, so Δf was calculated for different H. Since the FMR frequency is dependent on the confinement of the cuboid, it was obtained numerically by applying a spatially constant temporal field pulse for different H.
It is important to emphasize that in this small YIG film the demagnetization fields lower the effective field in the film significantly. One analytical source [Ulr] states for the used parameters a lowering of the external applied field of 10mT. A numerical examination pointed out that an external field of $H_{ext} = 65\text{mT}$ causes an internal field of $H_{int} = 46.32\text{mT}$, so even a higher decrease was observed. As the calculations were done with the dispersion relation for an infinite film, this effect had to be taken into account.

4.2.3 Damping

The actual damping $\alpha = 10^{-4}$ in YIG is very small. Accordingly, as the spin waves are damped very slowly in experiments, this material enables favourable experimental conditions. In simulations, however, the disadvantages predominate due to very long transients. Hence, the damping was raised artificially to $\alpha = 10^{-3}$ which had no significant effect on the processes apart from making them faster. Moreover, the various non-linear processes scale

differently with α, so the increased threshold fields led to a bigger interval in which only the first instability arose.

4.3 Simulation Output and Fourier Transforms

The first output of the mumax simulations was a tabular consisting of the time, the magnetization components that are averaged over the whole cuboid and freely selectable parameters like the total energy, the internal field components, etc. as one can see in app. E.1. Due to a chaotic uniform and spin wave distribution at the edges of the film (cf. e.g. fig. 5.3(a)-5.3(d)), the magnetization components that were only averaged over the center of the cuboid were also saved. Therefore, merely a range of 8.55x8.55μm^2 was considered in which the modes were excited effectively.
The total energy in the table, however, did not provide any information on the energy distribution among the different modes. In order to determine the energy of the uniform or spin wave modes, the fourier spectrum $P(f)$ of the modes had to be generated. Afterwards, the selection of and integration over the desired peak at its specific frequency led to its fourier energy $E(f)$.
As a consequence, another output of the simulations was the spatial distribution of the magnetization in the y=16 layer as implemented due to limited disc space. For a frequency resolution in the fourier spectrum of $\Delta f = 1/T = 0.1$GHz and a frequency range of $f = [0, 1/2 \cdot f_{sampling}] = [0, 1/2 \cdot 10]$Ghz $= [0, 5]$Ghz, a number of $N = f_{sampling} \cdot T =$ 10GHz$\cdot$100ns $= 1000$ magnetization distributions were saved covering a period of $T = 100$ns.
A temporal fourier transform of the oscillating out-of-plane (y) component of the 1000 saved magnetization distributions created fourier maps consisting of the local fourier amplitudes (real part, imaginary part and absolute value). If one for example considers a coherent excited mode with several nodes (mn) and frequency f_{mn}, then the fourier map concerning the frequency f_{mn} displays the spatial structure of this mode. Thus, one can display the absolute value of the wave distribution as shown in fig. 5.1(a).
For the purpose of analysing the mode structure, the complex amplitude of the fourier maps was transformed using a spatial fourier transformation. This method was required to establish the spatial wave vector as exemplary shown in fig. 5.4(a). The order in which the temporal and spatial fourier transforms were applied did not matter, since all information was conserved.
In contrast, the information of the fourier maps is reduced if the whole fourier spectrum of the magnetization is ascertained, i.e. the data is processed to display it compactly. Therefore, for every frequency map the global sum of the local, squared absolute values $A^2(x, z, f_i)$ was added up to gain the total fourier power $P(f_i)$ of the i^{th} frequency:

$$P(f_i) = \sum_{x,z} A^2(x, z, f_i). \tag{4.1}$$

To conclude, the whole mathematical calculation that was performed to obtain the complete spectrum $P(f)$ can be outlined in a simple way: $M(r,t) \rightarrow A(r,f) \rightarrow P(f)$.

4.4 Simulation Methods

4.4.1 Einstein de Haas Effect

In the previously presented adjusted experimental design similar to the Einstein de Haas experiment, the considered cuboid was a YIG film with a volume of $(100 \cdot 10 \cdot 100)\mu$m. Due to already mentioned reasons, a smaller cuboid with a volume of $(38.4 \cdot 5.12 \cdot 38.4)\mu$m was simulated. However, as this extension is roughly half of the one in the gedankenexperiment, the results may not be the same but at least similar for this larger volume.
First of all, the demagnetization factors N_i had to be determined numerically, because the ideal case of $N_x = N_z = 0$ and $N_y = 4\pi \cdot 10^{-7}$ for an infinite film is not given in the numerical considerations due to the finite extension of the cuboid in z and x direction. As these factors are only spatially constant in ellipsoids, one had to incorporate effective demagnetization factors for more complex shapes. The demagnetization factors describe the reduction of the internal magnetic field due to dipolar fields occurring because of the divergence of the magnetization:

$$H_{int,i} = H_{ext,i} - N_i M_i. \tag{4.2}$$

Since it is relatively easy to determine the internal magnetic field, the demagnetization factors could be calculated directly.
The next step was to apply uniform precession due to its highest ellipticity. As described in the theory, an external stimulus exciting the precession was needed for this purpose, which was in this case a dynamic magnetic field exciting the FMR mode of the sample: $\omega_p = \omega_{FMR}$. Here, the case for $\alpha = 0$ and a small initial magnetization deflection is equivalent to the case for $\alpha > 0$ and a small dynamic field, because in the latter case the pumping compensates the damping losses and therefore enables the same dynamic equilibrium.
The simulations finally delivered the values of the parameters needed for the calculation of the YIG film precession amplitude. A detailed explanation of the simulation method for exciting uniform precession is given in the next chapter.

4.4.2 Splitting Factor of Three-Magnon Splitting Process

As already explained in sec. 2.3.2, the splitting factor of three-magnon splitting should be <2 when incorporating the dipolar interaction into the spin wave model, because a part of the spin is carried by the lattice. In the simulations that will be presented in this subsection, this splitting factor will be determined.
The simulation method was based on a separate excitation of the uniform and the spin wave modes subsequently leading to a comparison of the obtained magnetizations and energies of these modes.
The direct excitation of the spin waves was done with a field that consisted of the static field $\boldsymbol{H} = H\boldsymbol{e}_z$ and a dynamic field $\boldsymbol{h}(z,t) = h(z,t)\boldsymbol{e}_x$ that was both temporally and spatially periodic:

$$\boldsymbol{H}_{tot}(z,t) = \boldsymbol{H} + \boldsymbol{h}(z,t) = H\boldsymbol{e}_z + h_0\boldsymbol{e}_x \cdot sin(k_z z) \cdot sin(2\pi f_{SW} t).$$

The dynamic field was modulated in the direction z of the static field, so that backward volume modes were excited with $\boldsymbol{k} \parallel \boldsymbol{H}$. It was applied in x direction to ensure perpendicular pumping being most effective in in-plane direction, because the in-plane magnetization $\boldsymbol{m}_x$ is larger than the out-of plane magnetization $\boldsymbol{m}_y$.
The excitation of this mask (cf. exemplary script in sec. E.1) takes place with the smallest allowed spin wave frequency to enable optimal efficiency.
In order to determine the wave vector k_z of the spin waves, further simulations had to be done: Three-magnon splitting processes were conducted by pumping energy into the FMR with a spatially homogeneous and temporal periodic field $\boldsymbol{h}(t) = h_0\boldsymbol{e}_x \cdot sin(2\pi f_{FMR} t)$. To enable this splitting process, the inequality $h_0 > h_{thr,1}$ had to be fulfilled, where $h_{thr,i}$ were the threshold fields of the different instabilities. The derivation of this threshold field $h_{thr,1}$ of the first-order instability process can be found in app. B. Subsequent to the simulations, the described temporal and spatial fourier transforms of the resulting magnetization distributions were accomplished and yielded the desired wave vector (cf. fig. E.2(a)-E.2(d) in app. E).
Lastly, the fourier energy of this spin wave mode was established as a function of the $\boldsymbol{h}$ field and the magnetization decrease ΔM_z (cf. sec. 2.4). Afterwards, this energy was compared to the energy of the FMR mode of uniform precession. The excitation of uniform precession was implemented in simple simulations taking a dynamic field $\boldsymbol{h}(t) = h_0\boldsymbol{e}_x \cdot sin(2\pi f_{FMR} t)$ with the same h_0 as in the case of spin wave excitation. Care had to be taken to keep this field smaller than the threshold field of the three-magnon splitting: $h_0 < h_{thr,1}$.

Chapter 5

Results & Discussion

5.1 Optimal Simulation Parameters

First of all, an optimal external static field of $H_{ext} = 65.26\text{mT}$ was calculated. However, due to possible analytical inaccuracies the field in the simulations was chosen to be slightly smaller, i.e. $H_{ext} = 65\text{mT}$. The resonance frequency $f_{FMR} = 3.26\text{GHz}$ was obtained numerically, yielding to a spin wave frequency of $f_{SW} = 1.63\text{GHz}$.
The demagnetization factors of the YIG film were determined to be $N_x = 1.50 \cdot 10^{-7}$, $N_z = 1.48 \cdot 10^{-7}$ and $N_y = 9.74 \cdot 10^{-7}$. These factors do not only agree with the theoretical expectation that $N_y >> N_x \approx N_z$ but also with $N_x + N_y + N_z = 12.72 \cdot 10^{-7} \approx 4\pi \cdot 10^{-7}$. Furthermore, the resulting internal field $H_{int,z} = 44.60\text{mT}$ for $H_{ext,z} = 65\text{mT}$, that was calculated via eq. 4.2, is in good agreement with the numerically obtained $H_{int,z} = 46.32\text{mT}$.
The threshold field for the three-magnon process was calculated to $h_{thr,1} = 9.4 \cdot 10^{-6}\text{mT}$ for a YIG damping of $\alpha = 1 \cdot 10^{-4}$, and to $h_{thr,1} = 9.4 \cdot 10^{-4}\text{mT}$ for the artificially higher damping of $\alpha = 1 \cdot 10^{-3}$. The wave vector of the spin waves created in the three-magnon process was determined to $k_z = 5.236 \frac{1}{\mu\text{m}}$.

5.2 Einstein de Haas Effect

As described in the theoretical chapters (eq. 2.18 and 3.14), the YIG film has an oscillation amplitude of

$$y_0 = \frac{l_1}{2} \cdot \left(\frac{\Delta m V}{2 J \omega_p \gamma} \right), \qquad \text{where} \qquad \Delta m = \frac{m_x^2}{4 M_0} \left(1 - \frac{m_y^2}{m_x^2} \right).$$

m_x^2 and $\frac{m_y^2}{m_x^2}$ can be either analytically determined via eq. 2.23 and 2.19 or alternatively numerically obtained by plotting the magnetization components of the mumax tables (cf. sec. 4.3). However, even the analytical approach bases on numerical parameters as the demagnetization factors of a real cuboid with finite extension cannot be calculated analytically.
In tab. 5.1, the analytical and numerical parameters and resulting amplitudes are presented for a comparison of the analytical calculations and the simulation. These parameters were calculated for a dynamic field of $h_0 = 2\,(4) \cdot 10^{-4}\text{mT} < h_{thr,1}$. The external field $H = 65\text{mT}$ was taken into account for the analytically derived values of m_x, $\frac{m_y}{m_x}$ and y_0 because the formulas used incorporated the confinement of the cuboid and the resulting attenuated static field. In order to determine the numerically derived y_0, the internal field $H = 46.32\text{mT}$ was considered. The reason is that the parameters m_x, m_y and $\frac{m_y}{m_x}$ used to calculate the numerical value for y_0 are functions of the effective internal field. In the numerical case, m_x and m_y were obtained and $\frac{m_y}{m_x}$ could be derived from this values. In contrast, analytically m_x and $\frac{m_y}{m_x}$ could be calculated and m_y was deduced from these two values.

Tab. 5.1 Comparison of analytically and numerically determined values for $H = 65\text{mT}$ and $h_0 = 2\,(4) \cdot 10^{-4}\text{mT}$.

Quantity	**Analytical Value**	**Numerical Value**
m_x [A/m]	134.0 (268.0)	107.1 (214.4)
m_y [A/m]	80.7 (161.5)	64.1 (128.3)
$\lvert a_0 \rvert$ [A/m]	$11.23\,(22.47) \cdot 10^{-4}$	$8.97\,(17.94) \cdot 10^{-4}$
$\frac{m_y}{m_x}$ [ ]	0.602 (0.602)	0.598 (0.598)
y_0 [m]	$2.50\,(10.01) \cdot 10^{-22}$	$1.63\,(6.54) \cdot 10^{-22}$

To discuss the obtained results, several aspects can be concluded:
To begin with, the proportionalities $m_x, m_y, |a_0| \propto h_0$ can be deduced from the eq. 2.23, 2.19 and 2.21 and are in accordance with the simulation results. Moreover, the proportionality $y_0 \propto h_0^2$ can be understood when expanding y_0 (eq. 3.13) for small arguments of the sine. Then, a proportionality $y_0 \propto m_x^2$ follows.
Furthermore, the validity of the formula for the ratio $\frac{m_y}{m_x}$ for the simulated dynamic fields h_0 has to be checked as it is only given for small h_0. In the orders of magnitude of $h_0 = 10^{-4}\text{mT}$ these ratios obtained for different h_0 fields differed only in the fourth decimal place, which means that the approximation for a negligible small deflection of the magnetization from its static equilibrium position is reasonable.
In a comparison of the analytically and numerically obtained values, small deviations are

noticed. As the analytical results appear to be constantly higher than the numerical ones, one can indicate that even the inclusion of the demagnetization factor and the internal field, respectively, could not facilitate an appropriate correction of the formulas for an infinite film. For example, the wave vector of the uniform precession cannot exactly equal zero for a film of finite extension. In such a system, no propagating waves but only standing waves exist with $k_{x,y} = \frac{m \cdot \pi}{l_{1,2}}$. The smallest wave number $k = \frac{\sqrt{2} \cdot \pi}{l_{1,2}} = 0.116 \frac{1}{\mu \mathrm{m}}$ is formed by $m = n = 1$, i.e. does not equal zero. Therefore, the theoretical approximation of an ideal uniform precession can be assumed to cause small deviations.
Furthermore, the analytically obtained values for the uniform precession amplitude $|a_{0,an.,1}| = 11.23\,(22.47) \cdot 10^{-4}$, that was calculated with the model incorporating the demagnetization factors, deviates from the value taken from eq. 2.21, $|a_{0,an.,2}| = 13.00\,(26.00) \cdot 10^{-4}$, that was determined for an infinite film with the use of the internal static field. Again, both results are higher than the numerically determined amplitude of $|a_{0,num.}| = 8.97\,(17.94) \cdot 10^{-4}$. Moreover, the numerically and analytically obtained resonance frequencies are not the same, even if the demagnetization factors were considered in the analytical derivation. Numerically, the resonance frequency was determined to $f_{FMR} = 3.26\mathrm{GHz}$. Analytically, a smaller FMR frequency of $f_{FMR} = 3.04\mathrm{GHz}$ followed.

The major result is that the obtained precession amplitude y_0 can be assumed to be too small to measure it in an experiment. This assumption is based on a comparison of the amplitude $y_0 \approx 10^{-21}\mathrm{m}$ with the sizes of e.g. an atom $\approx 10^{-10}\mathrm{m}$ or a proton $\approx 10^{-15}\mathrm{m}$. In the introduced adjusted experimental design that ought to be realized experimentally, it would be even smaller than in the simulations because a littler film was used that has a smaller moment of inertia.

5.3 Splitting Factor of Three-Magnon Splitting Process

In the following, the results of the excitation of uniform precession will be presented. Fig. 5.1(a) shows the spatial magnetization distribution of the whole simulated film. The typical distribution of a uniform mode can be identified, and furthermore some caustic waves that are normally positioned at the surfaces of a film. The related averaged upper (blue) and lower (green) halves of this distribution is presented in fig. 5.1(b) and show that the uniform precession is not effectively excited at the edges of the film. As a consequence, in fig. 5.1(c) and 5.1(d) the 57 cells in the middle of the film were extracted to present the same quantities in an area of a relatively homogeneous internal field.

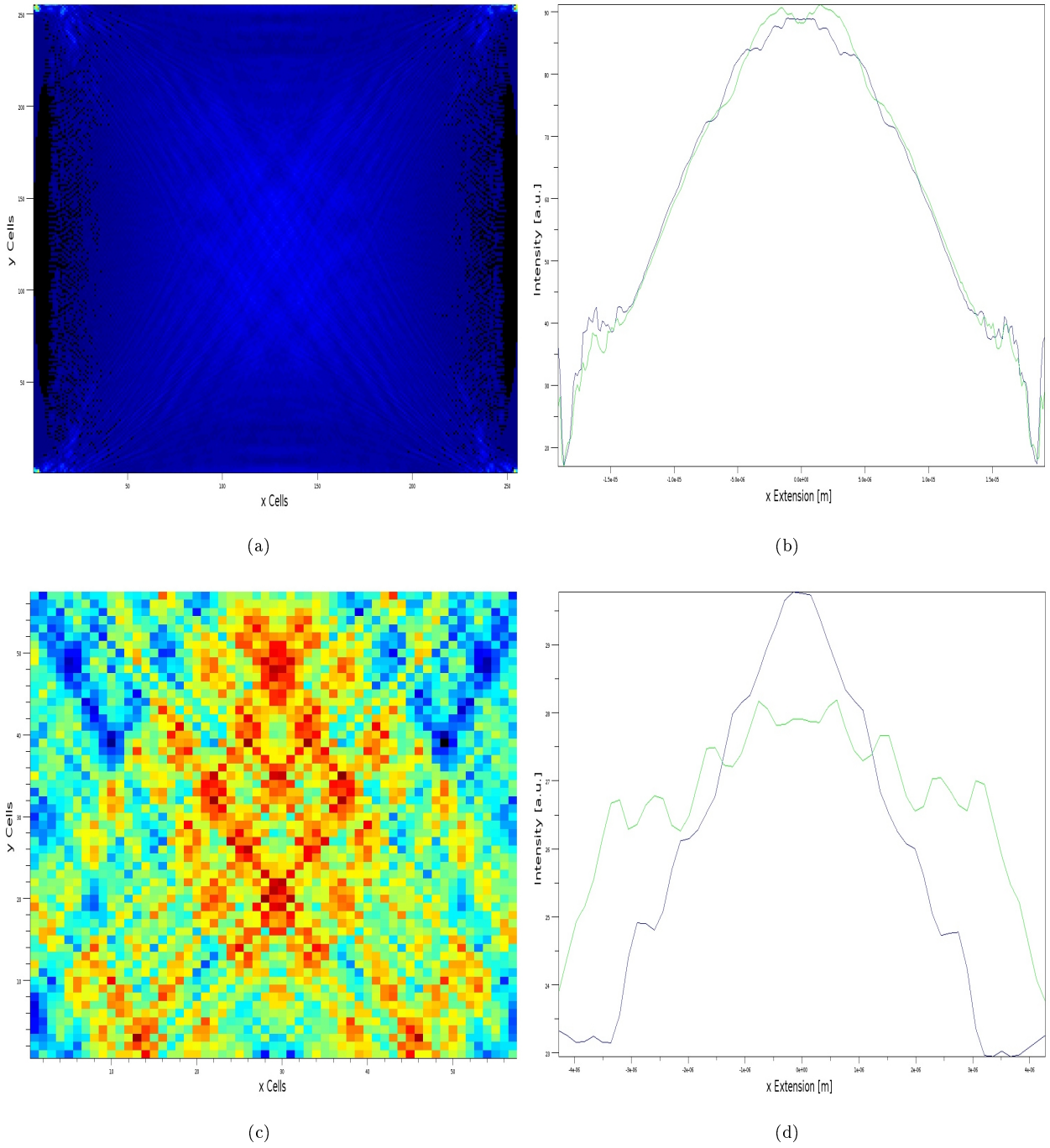

(a) (b)

(c) (d)

Fig. 5.1 Magnetization distribution of uniform precession excited with $h_0 = 4 \cdot 10^{-4}$mT. (a) Spatial magnetization distribution in the cells 0-256. (b) Averaged upper (blue) and lower (green) half of the spatial magnetization distribution in the cells 0-256. (c) and (d) show the same quantities, for the cells 100-156, i.e. the 57 cells in the middle of the film.

After transforming the cells 100-156 of the second magnetization component using a spatial fourier transformation, one obtained the spatial fourier spectrum as shown in fig. 5.2(a). When regarding the cross section $k_x = 0$, one obtained a single intensity peak around $k_z = 0$ as theoretically expected.

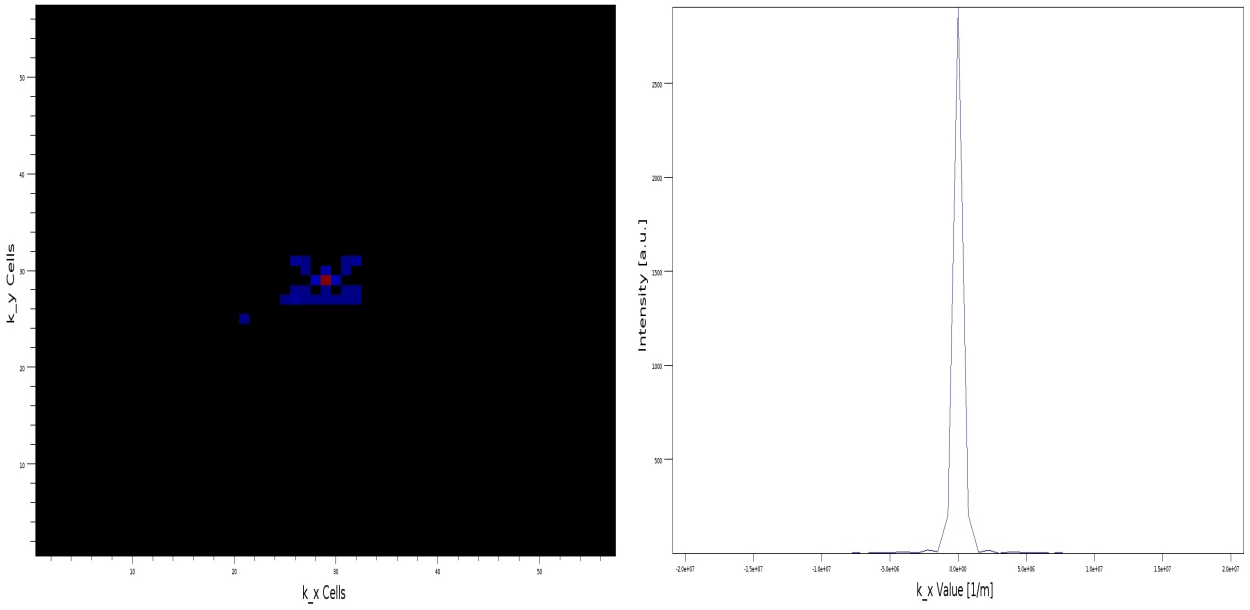

(a) (b)

Fig. 5.2 Spatial fourier transform of uniform precession excited with $h = 4 \cdot 10^{-4}$mT. (a) Spatial fourier spectrum and (b) cross section $k_x = 0$ of the spatial fourier spectrum, both in the 57 cells in the middle of the film.

The magnetization distributions of the spin waves excited with a temporally and spatially periodic dynamic field (cf. fig. 5.3(a) and 5.3(b)) suggests that it only gets effectively excited in the middle of the film, even more than in the case of uniform precession.
The actual wavelength of the spin wave is twice as large as in the presented distributions because the absolute value was plotted instead of the real magnetization distribution. For a comparison, the real and absolute values of this magnetization distribution can be seen in the appendix E in fig. E.4(a)-E.4(d).

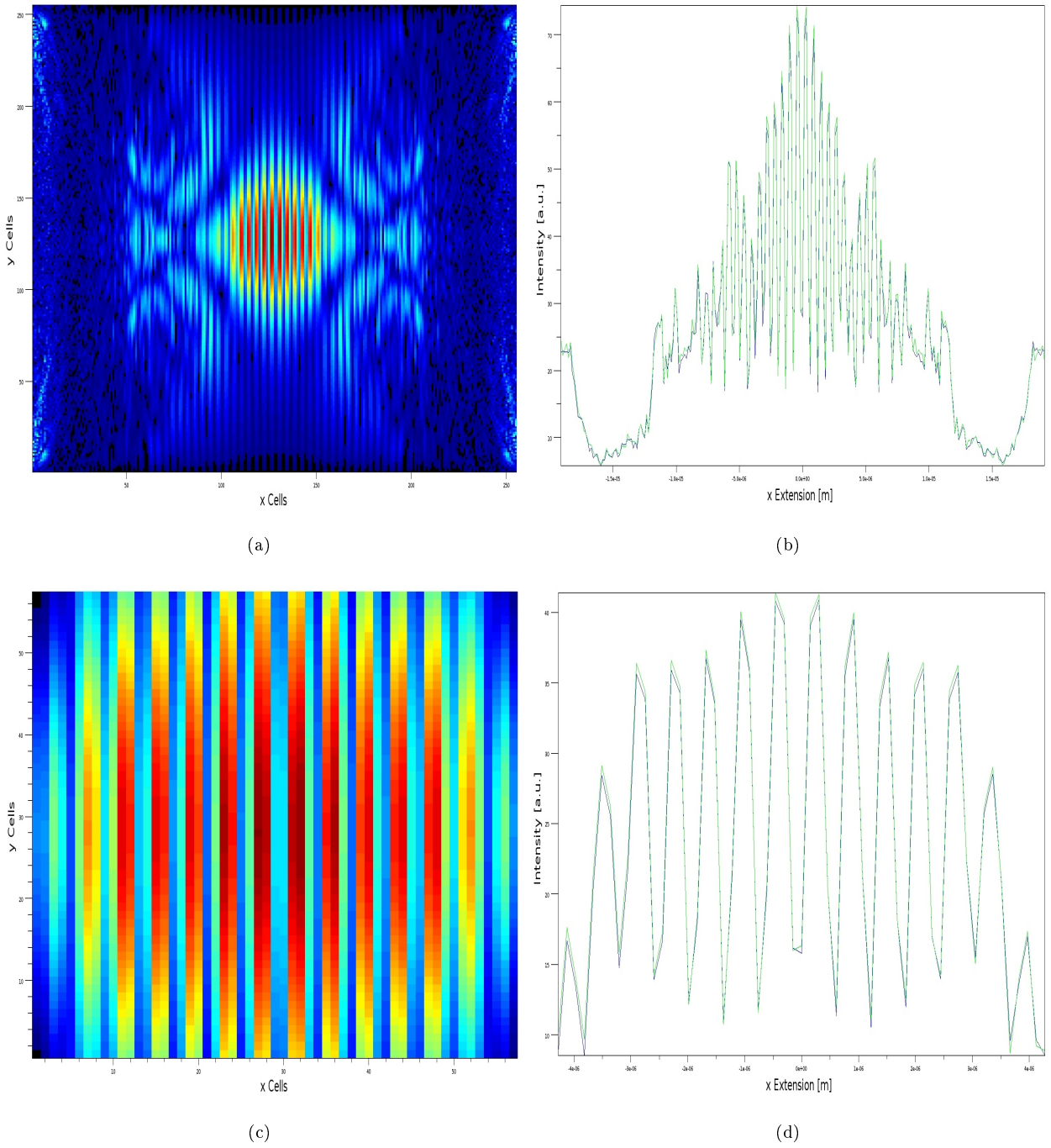

(a) (b)

(c) (d)

Fig. 5.3 Magnetization distribution of spin waves excited with $h_0 = 4 \cdot 10^{-4}$mT. (a) Spatial magnetization distribution in the cells 0-256. (b) Averaged upper (blue) and lower (green) half of the spatial magnetization distribution in the cells 0-256. (c) and (d) show the same quantities, for the cells 100-156, i.e. the 57 cells in the middle of the film.

The cross section of the spatial fourier spectrum of the cells 100-156 of the magnetization distribution (fig. 5.4(a)) yielded the value of $k = k_z = 5.236\frac{1}{\mathrm{m}}$ that was already part of the dynamic field mask. Again the fourier profile agrees with the theoretical expectation represented by iso-frequency curves in the k_x, k_z phase space as illustrated in [Ulr14, p. 21]. As the k vectors are nearly symmetric around zero, they describe standing waves.

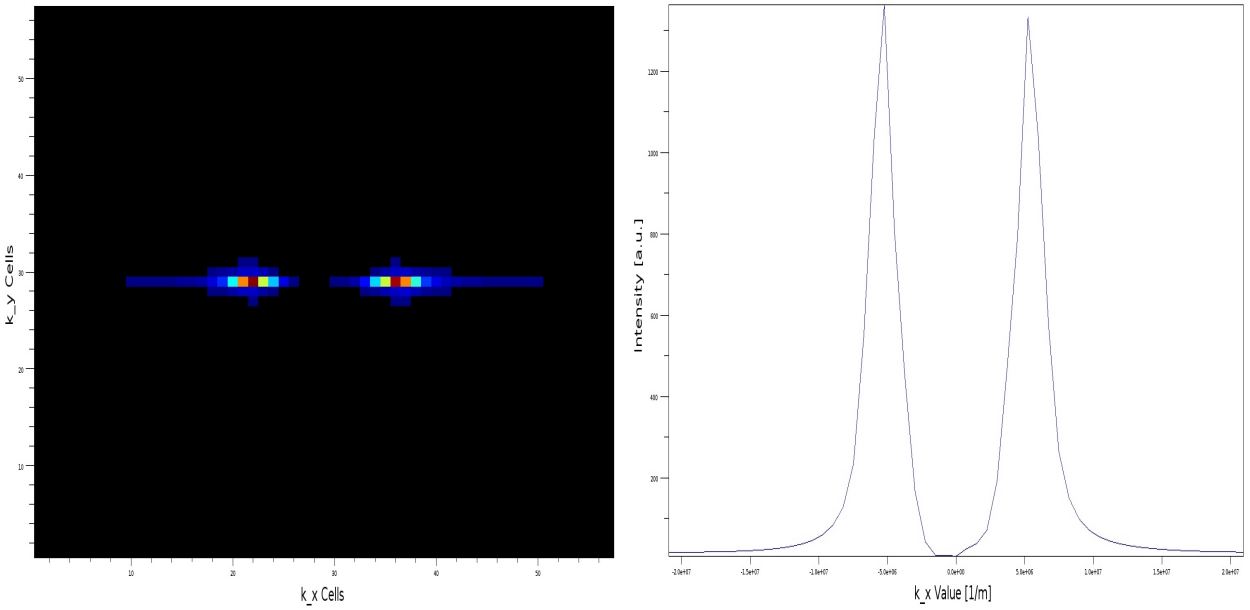

(a) (b)

Fig. 5.4 Spatial fourier transform of spin waves excited with $h_0 = 4 \cdot 10^{-4}$mT. (a) Spatial fourier spectrum and (b) cross section $k_x = 0$ of the spatial fourier spectrum in the 57 cells in the middle of the film.

Finally, the fourier energies of uniform precession and spin waves was obtained as a function of the static magnetization change $\Delta M_z = M_z(h_0 = 0) - M_z(h_0)$. The evidence that the fourier energy is proportional to the actual energy of the mode is given by the fact that the integral over the whole fourier spectrum is proportional to the total energy of the system deduced from the mumax output tables.
Fig. 5.5, where the data points refer to dynamic field strengths of $h = 0 - 8 \cdot 10^{-4}$mT, indicates that this relationship is linear. Furthermore, $E(\Delta M_z = 0) = 0$ is given for $h_0 = 0$ because only the perpendicular dynamic field decreased the static magnetization component parallel to the static field.

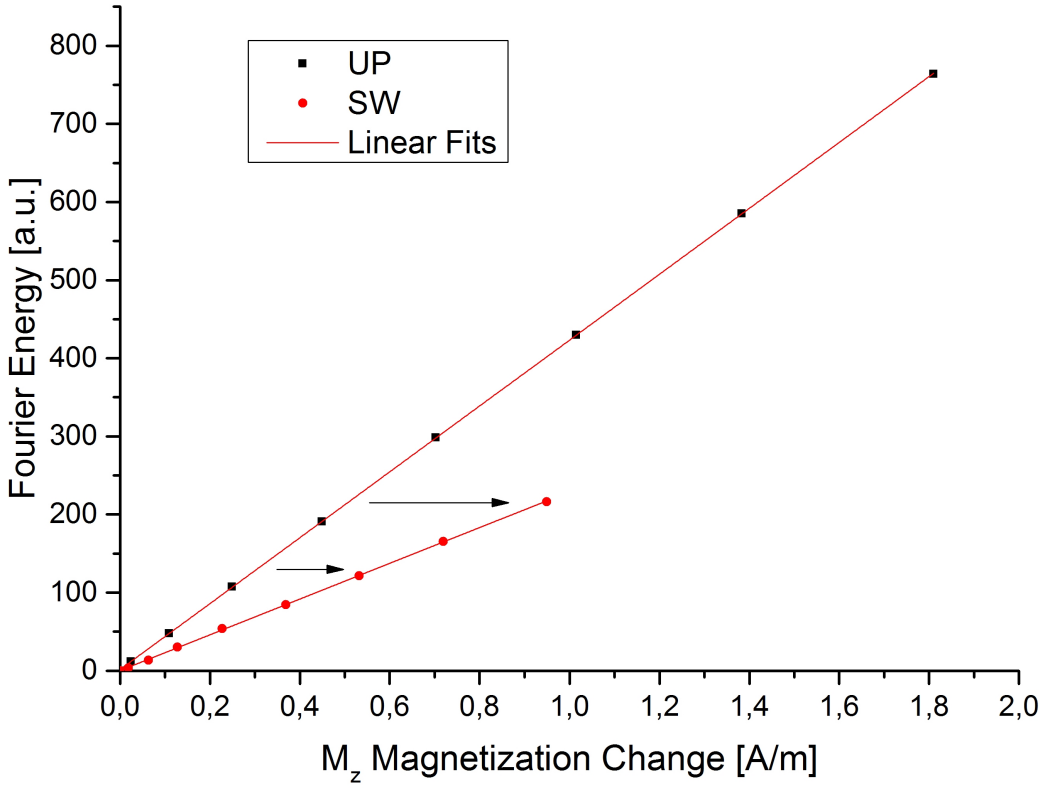

Fig. 5.5 Fourier energies of uniform and spin wave modes as a function of the static magnetization change ΔM_z parallel to the static field. The data points refer to dynamic field strengths of $h_0 = 0 - 8 \cdot 10^{-4}$mT.

As the optimal static field H could not be determined very accurately, the mask exciting the spin waves was potentially not perfectly matching and therefore not of optimal effectivity, as one can deduce from the lower spin wave fourier energies. However, by cancelling out the energy dependency on the dynamic field, results were obtained that were independent of the effectiveness of excitation with this approach.
As indicated by the arrows in fig. 5.5, the splitting factor is of interest, that describes how much magnetization change corresponds to the splitting of the uniform mode into two spin waves. Looking at the two equations of the linear fits

$$E_{UP}[a.u.] = (1.53 \pm 0.39)[a.u.] + (421.65 \pm 0.44) \cdot \Delta M_{z,UP} \cdot [m/A], \tag{5.1}$$
$$E_{SW}[a.u.] = (0.20 \pm 0.54)[a.u.] + (228.79 \pm 1.17) \cdot \Delta M_{z,SW} \cdot [m/A], \tag{5.2}$$

one sees that the slope for uniform precession is roughly twice as large as the one for spin waves. However, this splitting factor does not exactly equal 2, but:

$$\text{Splitting factor} = 1.84 \pm 0.01.$$

If one fixates the data point (0,0) in the linear fits, the slopes are 422.90 ± 0.51 for uniform precession and 229.10 ± 0.76 for spin waves. Here, a splitting factor of 1.85 ± 0.01 results.

Based on these results, one has to conclude that the simple quantization scheme of magnons with a magnetic moment of $2\mu_B$ and spin 1 cannot be confirmed. Instead, the conjecture stated in the supplementary information (p.7) of [KDD+11] gets affirmed: The uniform mode does not split into two magnons having spin 1. The secondary magnons rather carry spins that are smaller by 0.92 than the spin of the initial magnon with $k = 0$.
The magnetic moment of quasi-particles is defined as [KPS97, p. 187]

$$\boldsymbol{\mu}_{q.p.} = -\hbar \frac{\partial \omega_0}{\partial \boldsymbol{H}} \tag{5.3}$$

and the spin can be calculated to

$$\boldsymbol{s}_{q.p.} = \frac{\partial \omega_0}{\partial \omega_{\boldsymbol{H}}}. \tag{5.4}$$

Hence, the evaluation of the Kittel formula (eq. 2.7) and the numerically obtained frequencies result in a magnetic moment of $2.50\mu_B$ and a spin of 1.25 for the uniform mode. As a consequence of the splitting factor, the magnetic moments of the secondary spin waves have to equal $2.30\mu_B$ and their spin is 1.15. These values apply only to the specific chosen magnetic field and film extension. In general, the spins can be both higher and lower than 1, as described e.g. in [NB14, pp. 22-26].
These results that indicate a magnon spin $\neq 1$ are merely received in the case of incorporating dipolar energy (cf. e.g. [NB14, pp. 22-26]). Therefore, these determined spins of the uniform and the spin wave modes are only the magnetic parts of the total spin consisting of a magnetic and a lattice part (ref. [KDD+11]). This explanation is based on the necessity of the spin being integer 1 as the magnon is a boson, shown e.g. by its ability to conduct Bose Einstein condensation [DDD+06].
As already mentioned, a coherent quantum description of this phenomenon is still missing. This fact acts as a great motivation for further research potentially leading to a consistent description of the quantum mechanical properties of ferromagnet including exchange as well as dipolar interactions.

Chapter 6

Conclusion

To recapitulate, the current thesis provided a brief overview on several aspects of magnetic dynamic processes.
It was presented that in contrast to former estimations, the amplitude of the YIG film oscillation induced by the elliptic magnetization precession is too small to be measured in an experiment. Furthermore, the violation of angular momentum conservation was illustrated as was already expected based on previous results. As the simulations resulted in an obtained three-magnon splitting factor of 1.84 instead of 2, the consequential magnon spin $\neq 1$ can only be described by the introduction of a total magnon spin consisting of a magnetic as well as a lattice part.
Since still no coherent quantum description of this phenomenon exists, it acts as a great motivation for further research aiming for a complete account of the quantum mechanical properties of a ferromagnet, incorporating exchange as well as dipole interactions.

Appendix A

Derivation of Oscillation Amplitude via Conservation of Angular Momentum

Another derivation of the precession amplitude of the YIG film was conducted by S. O. Demokritov and simply bases on the consideration of the angular momentum conservation,

$$\dot{\boldsymbol{L}}_{mag} + \dot{\boldsymbol{L}}_{mech} = 0. \tag{A.1}$$

As mentioned, the change of the magnetic angular momentum can be written as (eq. 3.5)

$$\dot{L}_{mag} = \frac{V\dot{M}_z}{\gamma} = \frac{V 2\omega_p \Delta m \sin(2\omega_p t)}{\gamma}. \tag{A.2}$$

With the precession angle $\varphi = \varphi_0 \sin(2\omega_p t)$ of the YIG film and the related angular velocity $\Omega = \dot{\varphi}$ one obtains an expression for the mechanical angular momentum and its derivative,

$$L_{mech}(t) = J\Omega = J2\omega_p\varphi_0 \sin(2\omega_p t) \qquad \text{and} \qquad \dot{L}_{mech}(t) = -J4\omega_p^2\varphi_0 \sin(2\omega_p t). \tag{A.3}$$

The conservation of angular momentum (eq. A.1) leads to

$$\frac{2\omega_p V \Delta m}{\gamma} \sin(2\omega_p t) - J4\omega_p^2\varphi_0 \sin(2\omega_p t) = 0, \tag{A.4}$$

and finally to expressions for the maximal oscillation angle and for the oscillation amplitude as already derived in sec. 3.4 (eq. 3.14):

$$\varphi_0 = \frac{\Delta m V}{2J\omega_p\gamma} \qquad \text{and} \qquad y_0 = \frac{l_1}{2} \cdot \varphi_0 = \frac{l_1}{2} \cdot \left(\frac{\Delta m V}{2J\omega_p\gamma}\right). \tag{A.5}$$

Appendix B

Calculation of Threshold Field of Three-Magnon Splitting

The threshold field for the first-order Suhl instability can be calculated to [GM96, p. 252]

$$h_{thr,1} = \frac{\Delta H_0 \Delta H_k}{\pi M_0} \tag{B.1}$$

with [GM96, p. 20]

$$\Delta H_{0,k} = \frac{2\omega_{r0,rk}}{\gamma}. \tag{B.2}$$

The frequency ω_r can be calculated to

$$\omega_r = \alpha\omega \frac{\partial\omega}{\partial\omega_H} \tag{B.3}$$

with the dispersion relation (cf. 2.8 [KS86, p. 6,7,10,55,60], [Kal80, p.5,6,9], diagonal approximation)

$$\omega = \sqrt{\omega_H \left(\omega_H + \frac{\omega_M}{kl_2}\left(1 - e^{-kl_2}\right)\right)}. \tag{B.4}$$

After differentiating ω (eq. B.4) with respect to ω_H we receive

$$\omega_r = \alpha \left(\omega_H + \frac{\omega_M}{2kl_2}\left(1 - e^{-kl_2}\right)\right), \tag{B.5}$$

hence, for ΔH_k follows

$$\Delta H_k = \alpha \left(2H + \frac{\mu_0 M_0}{k l_2} \left(1 - e^{-k l_2} \right) \right). \tag{B.6}$$

To receive ΔH_0 we can expand the exponential function in eq. B.4 for $k \to 0$ into a Taylor series to the first order and receive the Kittel formula for an infinite film [Kit48, p. 6]

$$\omega = \sqrt{\omega_H (\omega_H + \omega_M)}. \tag{B.7}$$

After differentiating ω (cf. eq. B.7) with respect to ω_H,

$$\omega_{r0} = \alpha \left(\omega_H + \frac{1}{2} \omega_M \right) \tag{B.8}$$

follows and therefore

$$\Delta H_0 = \alpha (2H + \mu_0 M_0). \tag{B.9}$$

Finally we obtain a threshold field for the Suhl instability of

$$h_{thr,1} = \frac{\alpha^2 (2H + \mu_0 M_0) \left(2H + \frac{\mu_0 M_0}{k l_2} \left(1 - e^{-k l_2} \right) \right)}{\pi M_0}, \tag{B.10}$$

so a proportionality of $h_{thr} \propto \alpha^2$ was derived. For the typical damping of YIG $\alpha = 1 \cdot 10^{-4}$, a threshold field of $h_{thr,1} = 9.4 \cdot 10^{-6}$mT followed. With the artificially higher damping of $\alpha = 1 \cdot 10^{-3}$ one receives a threshold field of $h_{thr,1} = 9.4 \cdot 10^{-4}$mT. This threshold field is of course only an approximation as the formulas for an infinite film were used.

Appendix C

Expansion of M_z for Small Dynamic Magnetization Components

The expression for the magnetization component parallel to the static field

$$\begin{aligned} M_z &= \sqrt{M_0^2 - m_x^2 \cos^2 \omega_p t - m_y^2 \sin^2 \omega_p t} \\ &= M_0 \cdot \sqrt{1 - \frac{m_x^2}{M_0^2} \cos^2 \omega_p t - \frac{m_y^2}{M_0^2} \sin^2 \omega_p t} \end{aligned} \tag{C.1}$$

shall be expanded for small dynamic amplitudes $\left|\frac{m_{x,y}}{M_0}\right| << 1$ into the more informative approximative term

$$M_z \approx M_0 - \frac{1}{4M_0}(m_x^2 + m_y^2) + \frac{1}{4M_0}(m_y^2 - m_x^2)\cos 2\omega_p t. \tag{C.2}$$

Therefore, one just considers terms up to the first order. For the zeroth order follows

$$M_z(0) = M_0. \tag{C.3}$$

For the first order, the Taylor term for the expansion points $\left(\frac{m_{x,y}}{M_0}\right)^2 = 0$ are

$$M_0 \cdot \frac{1}{2}(1-0-0)^{-\frac{1}{2}}(-\cos^2 \omega t)\left(\frac{m_x^2}{M_0^2} - 0\right) \tag{C.4}$$

$$M_0 \cdot \frac{1}{2}(1-0-0)^{-\frac{1}{2}}(-\sin^2 \omega t)\left(\frac{m_y^2}{M_0^2} - 0\right). \tag{C.5}$$

With the trigonometric relations

$$\cos^2 \omega t = \frac{1}{2}(1 + \cos 2\omega t), \;\; \sin^2 \omega t = \frac{1}{2}(1 - \cos 2\omega t) \tag{C.6}$$

finally the following desired informative approximative expression for M_z is obtained

$$\begin{aligned} M_z &= M_0 - \frac{1}{2M_0}\left(m_x^2 \cdot \frac{1}{2}(1 + \cos 2\omega t) + m_y^2 \cdot \frac{1}{2}(1 - \cos 2\omega t)\right) \\ &\approx M_0 - \frac{1}{4M_0}(m_x^2 + m_y^2) - \frac{1}{4M_0}(m_x^2 - m_y^2)\cos 2\omega t. \end{aligned} \tag{C.7}$$

Appendix D

Demonstration of Equality of Uniform Precession and Spin Waves for $k \to 0$

In [GM96, p. 184] it is stated that for spin waves the relation

$$\frac{m_y}{m_x} = -i\left(1 + \frac{\omega_M \sin^2\vartheta_k}{\omega_H + \eta k^2}\right)^{-\frac{1}{2}} = -i\left(\frac{A_k + |B_k|}{A_k - |B_k|}\right) \tag{D.1}$$

is given for arbitrary k-vectors. However, this expression contains a typing error and the correct relation is the following

$$\frac{m_y}{m_x} = -i\left(1 + \frac{\omega_M \sin^2\vartheta_k}{\omega_H + \eta k^2}\right)^{-\frac{1}{2}} = -i\left(\frac{A_k + |B_k|}{A_k - |B_k|}\right)^{-\frac{1}{2}}. \tag{D.2}$$

To show this equality, the case $k \to 0$ has to be considered for which this ratio has to transition into the expression for uniform precession ([GM96, p. 26] apart from the forgotten M_0)

$$\frac{m_y}{m_x} = -i\left(\frac{H + (N_y - N_z)\cdot M_0}{H + (N_x - N_z)\cdot M_0}\right)^{-\frac{1}{2}}. \tag{D.3}$$

Therefore, we have to consider the terms A_k and $|B_k|$ in eq. D.2:

$$A_k = \omega_H + l_{ex}^2\omega_M k^2 - \frac{1}{2}\omega_M(P_0(1 - \sin^2\vartheta_k) - 1), \tag{D.4}$$

$$|B_k| = \frac{1}{2}\omega_M(P_0(1 + \sin^2\vartheta_k) - 1), \tag{D.5}$$

where we can neglect the term $\propto k^2$. Finally, one has to Taylor expand P_0 for small k

$$P_0 = \frac{1 - e^{-kl_2}}{kl_2} \doteq \frac{1 - (1 - kl_2 - ...)}{kl_2} \approx 1. \tag{D.6}$$

and insert this expressions into the second term of eq. D.2:

$$\begin{aligned}
\frac{m_y}{m_x} &= -i \left(\frac{\omega_H - \frac{1}{2}\omega_M(1 \cdot (1 - \sin^2\vartheta_0) - 1) + \frac{1}{2}\omega_M(1 \cdot (1 + \sin^2\vartheta_0) - 1)}{\omega_H - \frac{1}{2}\omega_M(1 \cdot (1 - \sin^2\vartheta_0) - 1) - \frac{1}{2}\omega_M(1 \cdot (1 + \sin^2\vartheta_0) - 1)} \right)^{-\frac{1}{2}} \\
&= -i \left(\frac{\omega_H + \omega_M \sin^2\vartheta_0}{\omega_H + \frac{1}{2}\omega_M \sin^2\vartheta_0 - \frac{1}{2}\omega_M \sin^2\vartheta_0} \right)^{-\frac{1}{2}} \\
&= -i \left(1 + \frac{\omega_M}{\omega_H} \sin^2\vartheta_0 \right)^{-\frac{1}{2}}.
\end{aligned} \tag{D.7}$$

In comparison to eq. D.1 [GM96, p. 184] one can see that this relation contains the mistake of leaving out the exterior power of the fraction, as it exists in eq. D.7. This observation can be elucidated by further conversions of eq. D.7:

$$\frac{m_y}{m_x} = -i \left(1 + \frac{\gamma\mu M_0}{\gamma H} \sin^2\vartheta_0 \right)^{-\frac{1}{2}} = -i \left(\frac{H + \mu M_0 \sin^2\vartheta_0}{H} \right)^{-\frac{1}{2}}. \tag{D.8}$$

This expression is identical with the one for uniform precession:

$$\frac{m_y}{m_x} = -i \left(\frac{H + (N_y - N_z) \cdot M_0}{H + (N_x - N_z) \cdot M_0} \right)^{-\frac{1}{2}} \tag{D.9}$$

for $N_x = N_z = 0$ and $N_y = \mu \sin^2\vartheta_0 = 4\pi \cdot 10^{-7}$ due to $\sin^2\vartheta_0 = 0$ as the angle between $\mathbf{M}$ and $\mathbf{k} = 0$ is $\vartheta_0 = \pi/2$. These expressions for N_x, N_y, N_z are exactly the ones for the considered infinite film.

Appendix E

Commented Scripts and Data

E.1 Scripts

Exemplary mumax Script

The following script is an exemplary mumax script showing the simulation parameters and the output for excitation of spin waves with a spatially and temporally periodic h field mask.

```
SetGridsize(256, 256, 32)
SetCellsize(0.15e-6, 0.15e-6, 0.16e-6)
// Mumax convention -> thesis convention: (x,y,z) -> (z,x,y).

Msat  = 139261                  // Saturation magnetization in A/m.
Aex   = 3.614e-12               // Exchange constant in I/m.
alpha = 0.02
// Initial higher damping for faster relaxation of magnetization.

Bstatic := 65e-3                // Static field in T.
B_ext = vector(Bstatic, 0, 0)   // Static field applied in x(z) direct.
Bexc := 4e-7                    // Dynamic field in T.
f:=1.63e9                       // SW frequency f=f_FMR/2.

m=uniform(1,0,0)        // Initial magnetization parallel to static field.
relax()                 // Relaxation into static equilibrium.

OutputFormat = OVF1_TEXT        // File format of output is .ovf.

alpha = 1e-3            // After relaxation, correct damping is turned on.

mxcrop:=Crop(m, 100, 156, 100, 156, 15, 16)
// Only magnetization in the middle of the cuboid is saved,
// as only there the SW excitation is effective.

FixDt = 2.5e-11
// Integration time. Integration method: Bogacki Shampine method,
// one of Runge Kutta approximation methods.
```

```
tableautosave(5e-11)    // Every 5e-11 seconds all 3 magnetization comp. are saved.
tableAdd(E_total)       // Time evolution of total energy of system is added to table,
tableAdd(mxcrop)        // as well as magnetization in middle of the cuboid,
tableAdd(B_eff)         // and effective, internal field.

k1:=5.236e6                                     // k vector of the SW.
mask := newslice(3, 256, 256, 32)
// Create mask for spatially and temporally periodic dyn. field,
for i:=0; i<256; i++{                           // for all x cells,
    for j:=0; j<256; j++{                       // all y cells,
        for k:=0; k<32; k++{                    // and all z cells.

            r := index2coord(i, j, k)           // Creation of coordinates for field.
            x := r.X()                          // Only x coordinates important.
            B := Bexc*sin(k1*x)
            // Spatially periodic profile of dynamic field with SW k vector.
            mask.set(1, i, j, k, B)
        }   // Set mask for whole (i,j,k) coordinate system,
    }       // apply field in y(x)=1 direction.
}

B_ext.add(mask, sin(2*pi*f*t))
// Add temporally perdiodic (with SW frequency) mask to static field.
// To create UP and not SW, take not mask but
//B_ext = vector(Bstatic, Bexc*sin(2*pi*f*t), 0).

run(5e-7)
// Run simulation for 500ns until dynamic equilibrium is reached.
autosave(CropLayer(m, 16),0.1*1e-9)
// Save layer z(y)=16 magnetization comp. for every cell, every 0.1ns.
run(100e-9)
 // Run saving for 100ns so that 1000 magnetization profiles are saved.
```

Exemplary Scilab Script

In order to obtain the FMR frequencies for a range of different $\boldsymbol{H}$ fields to determine the optimal one for which $\Delta f = f_{FMR} - 2 \cdot f_{min} = 0$ is given, a dynamic field pulse was applied to the micromagnetic mumax sample for different static fields. The following exemplary Scilab script (mostly written by H. Ulrichs) presents the method to read out the FMR peaks and therefore acts as an exemplary script illustrating the different evaluation methods used in this thesis.

```
clear  // Clear all parameters
clf()  // and figures.

// Define Lorentz function for fitting FMR peaks.
function e=lor(p,z)
    x=z(1);
    y=z(2);
    e=y-p(1)*1/2*p(3)/%pi/((x-p(2))^2+1/4*p(3)*p(3));
endfunction

// Open and read table comprising time, magn. comp. and total energy.
filelocation='/home/mumax/simulation/Lena/256x256x32/find_FMR.out/table.txt';

a=mopen(filelocation, 'r');
b=mfscanf(11,a,'%s');

// Find frequency maxima = FMR
maxima=zeros(25,3);

for j=1:20 // For e.g. 20 maxima corresponding to 20 pulses with different H field

 data=zeros(10000,2);        // Matix "data" will have two components...

 for i=1:10000
    b=mfscanf(5,a,'%f');     // Define data as:
    data(i,1)=b(1);          // First column of table: time.
    data(i,2)=b(4);          // Fourth column of table: z(y) magn. comp.
 end

 deltaf=1/500;                                  // Frequency resolution.
 f=linspace(0,deltaf*(10000-1),10000);          // Frequency.

 // Fourier transform data to receive frequency spectrum.
 c=abs(fft(data(:,2)));

 // Plot frequency spectrum = fourier transformed data containing FMR peaks.
 subplot(211)
 plot(f,c);

 // Find maxima in frequency spectrum with
 [value,index]=max(c(1:5000))
 p0=[max(c);f(index);0.1];       // initial guess of maxima
 Z=[f(index-100:index+100)',c(index-100:index+100,1)]'
 // and Z=matrix [z1,...zn] where z_i is the ith simulation.

 // Fit FMR peaks with Lorentz function.
 [p,err]=datafit(lor,Z,p0);
```

```
 // Plot the Lorentz fits in spectrum.
 plot(f,p(1)*1/2*p(3)/%pi*((f-p(2)).^2+1/4*p(3)*p(3)).^(-1),'r')


 maxima(j,1)=60e-3+(0.5e-3)*i
 // Starting value of static field: H=60mT. End value: H=70mT.
 // 20 steps (=20 maxima) in a distance of 0.5mT.
 maxima(j,2)=p(2);
 maxima(j,3)=p(3);

 // Plot maximum = FMR frequency as a function of number of maximum (1-10).
 subplot(212)
 plot(j,p(2),'r.')

end
mclose();  // Close table.
```

E.2 Data

Exemplary Time Evolution of Magnetization Components of Uniform Precession

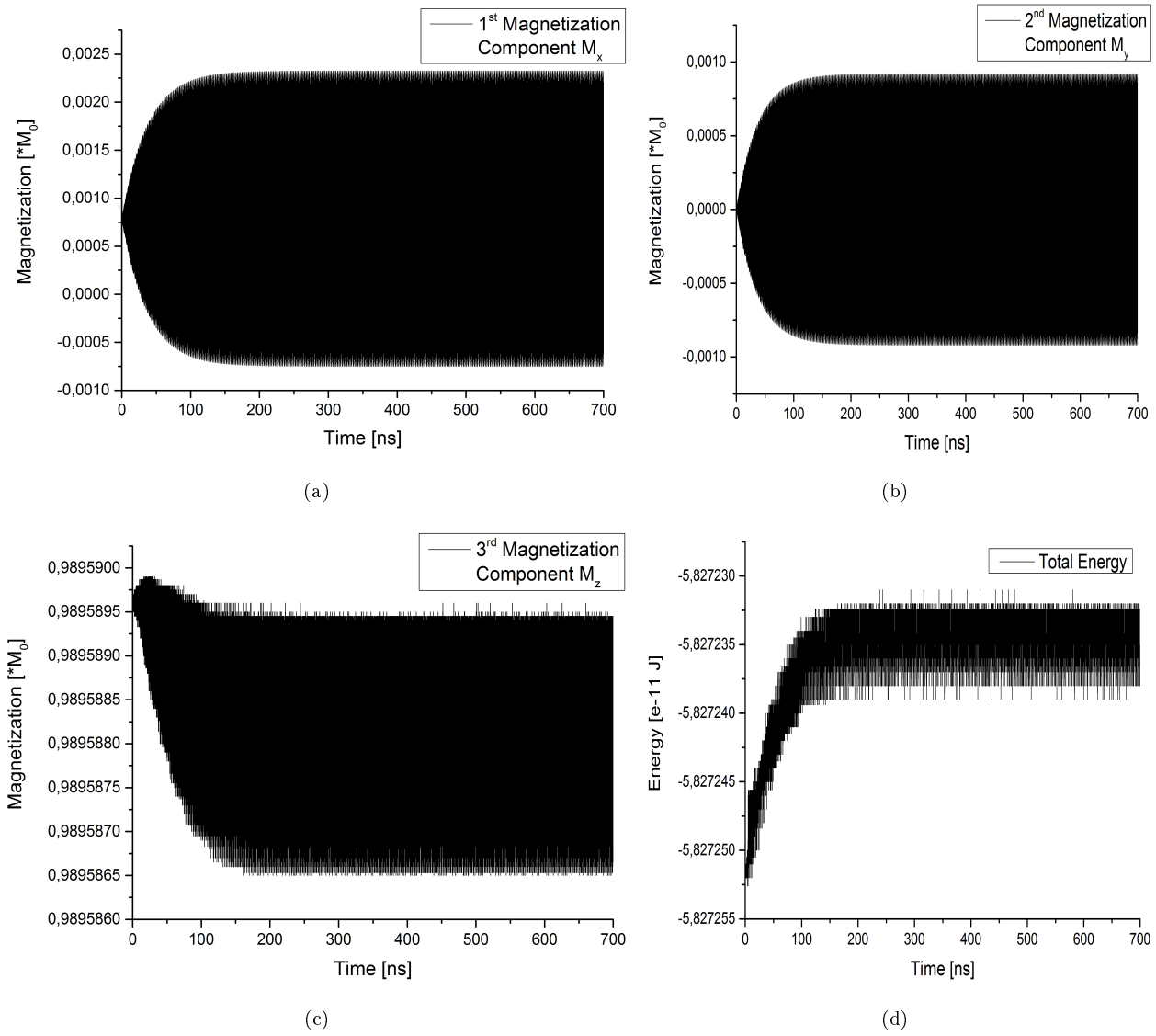

Fig. E.1 Exemplary time evolution of magnetization components of uniform precession excited with $h_0 = 4 \cdot 10^{-4}$mT. The (a) M_x in-plane component and (b) M_y out-of-plane component increase due to h_0. (c) The amplitude of the M_z component parallel to the static field first was saturated (cf. to hysteresis curve) but increased due to the perpendicular dynamic field until finally a dynamic equilibrium is obtained. (d) The total energy $E \propto -M_0 H$ increases as the scalar product $M_0 H$ gets smaller.

Ascertainment of k Vector of Spin Waves via Excitation with Pumping

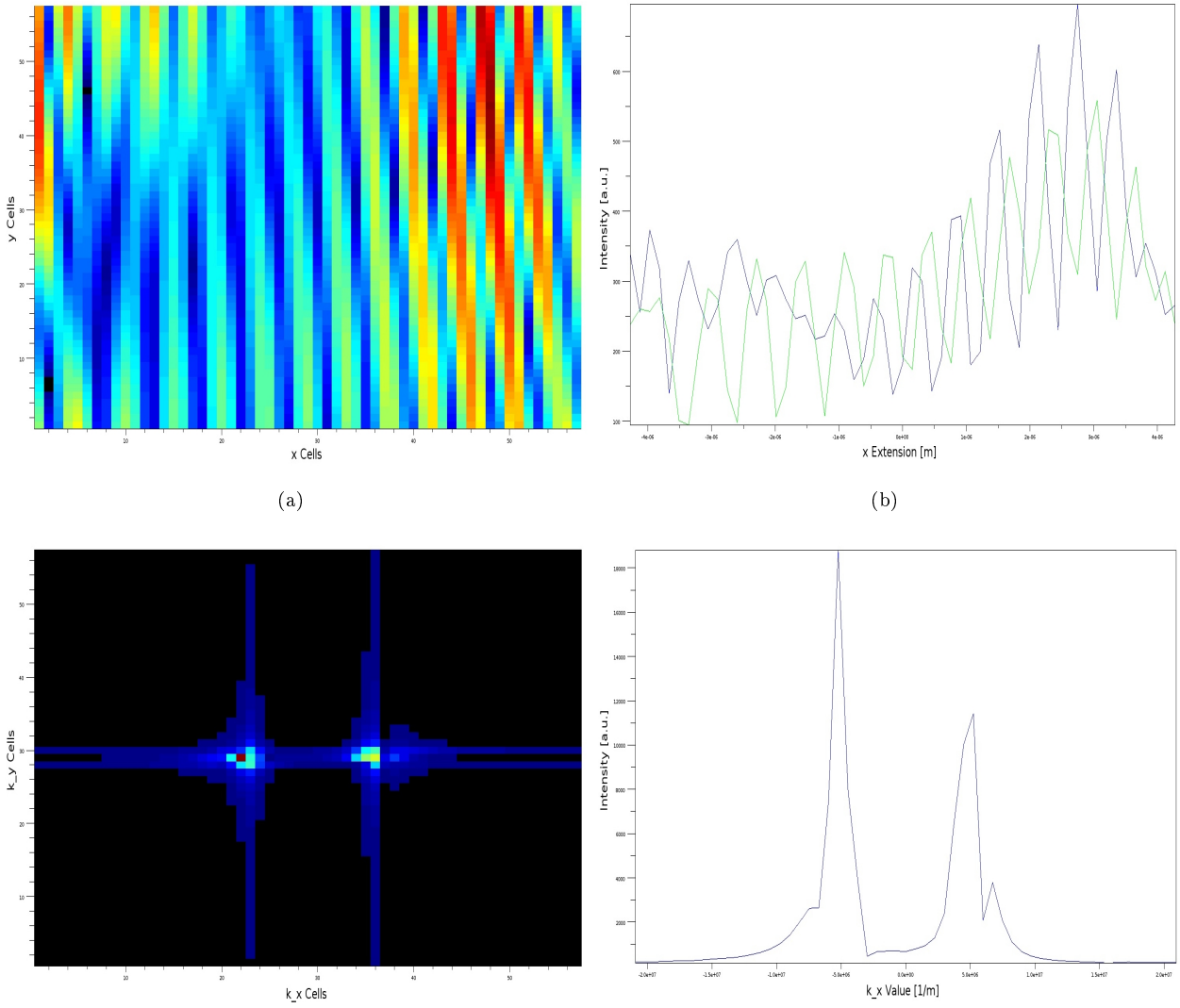

(a) (b)

(c) (d)

Fig. E.2 Ascertainment of k vector of spin waves via pumping with FMR frequency and $h_0 = 80 \cdot 10^{-4}$mT. Cells 100-156 of: (a) Spatial magnetization distribution. (b) Averaged upper (blue) and lower (green) half of the spatial magnetization distribution. (c) Spatial fourier spectrum. (b) Cross section $k_x = 0$ of the spatial fourier spectrum leading to $k_z = 5.236 \frac{1}{\mu\text{m}}$.

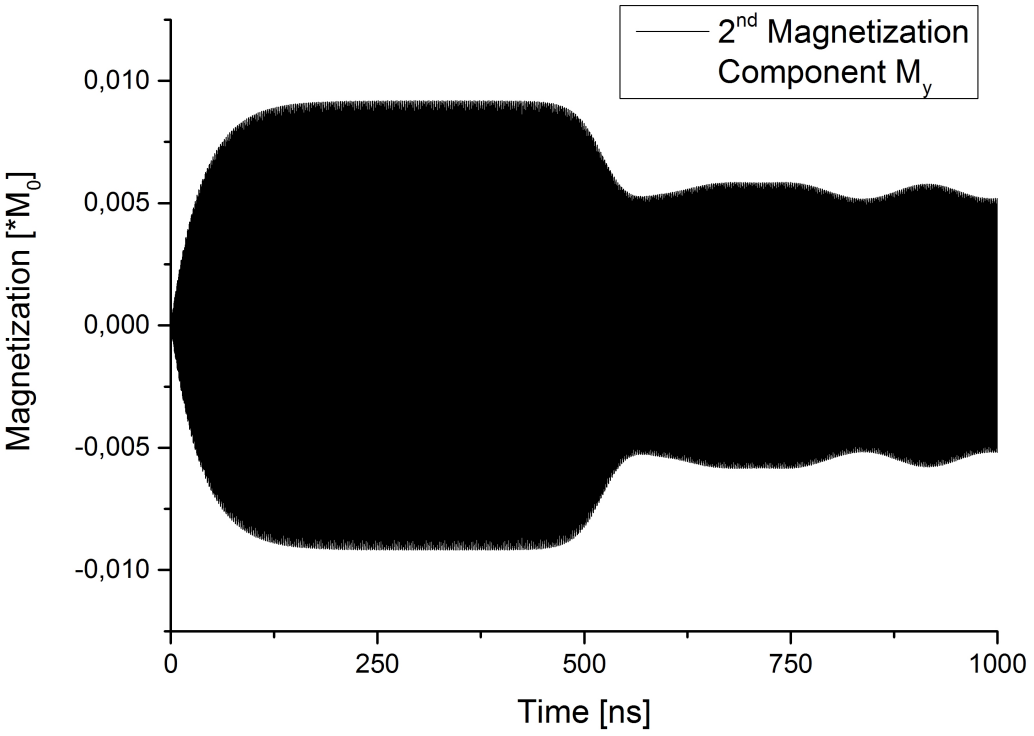

Fig. E.3 Time evolution of out-of-plane magnetization component for splitting process with $h_0 = 40 \cdot 10^{-4}$mT. After a transient of approximately 500ns, the splitting process starts.

Comparison of Absolute and Real Magnetization Distributions of Spin Waves

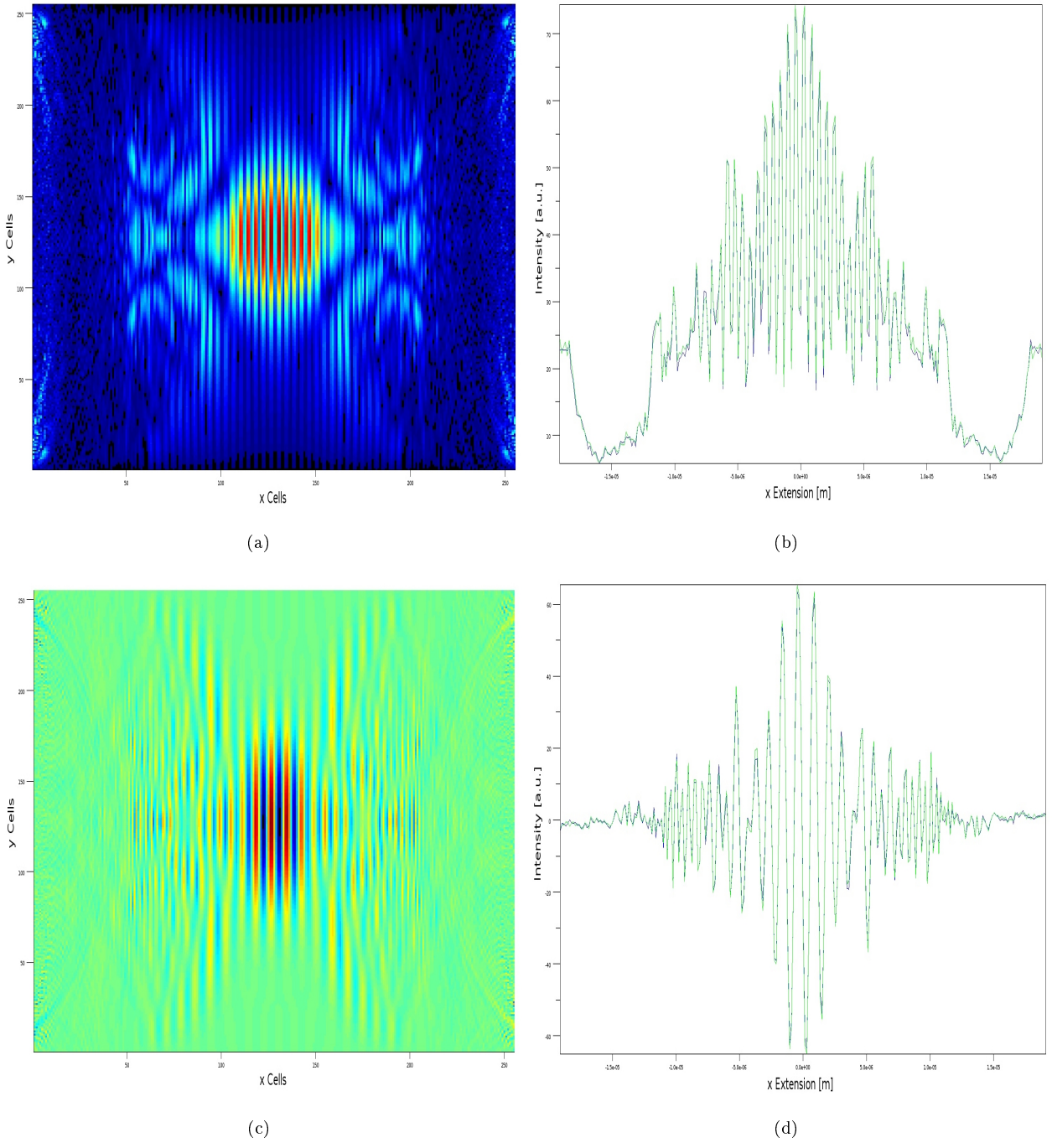

(a) (b)

(c) (d)

Fig. E.4 Comparison of absolute and real magnetization intensity distributions of spin waves excited with $h_0 = 4 \cdot 10^{-4}$mT. (a) Absolute values of spatial magnetization distribution in the cells 0-256. (b) Averaged upper (blue) and lower (green) half of the spatial magnetization distribution in the cells 0-256. (c) and (d) show the same quantities, but real instead of absolute values.

References

[ABP68] A. I. Akhiezer, V. G. Bar'yakhtar, and S. V. Peletminskii. *Spin Waves*. North Holland, Amsterdam, 1968.

[Blo30] F. Bloch. Zur Theorie des Ferromagnetismus. *Zeitschrift für Physik*, 61(3-4):206–219, 1930.

[BSPA59] N. Bloembergen, S. Shapiro, P. S. Pershan, and J. O. Artman. Cross-relaxation in spin systems. *Phys. Rev.*, 114:445–459, Apr 1959.

[Bur91] F. Burk. *Lebesgue Measure and Integration: An Introduction*. John Wiley and Sons, Wiley-Interscience, 1991.

[Cal05] A. Calaprice. *The Einstein Almanac*. Johns Hopkins University Press, Baltimore, 2005.

[DDD+06] S. O. Demokritov, V. E. Demidov, O. Dzyapko, G. A. Melkov, A. A. Serga, B. Hillebrands, and A. N. Slavin. Bose-Einstein condensation of quasi-equilibrium magnons at room temperature under pumping. *Nature*, 443(7110):430–433, 2006.

[De09] S. O. Demokritov (ed.). *Spin Wave Confinement*. Pan Stanford Publishing Pte. Ltd., Singapore, 2009.

[Dem94] W. Demtröder. *Experimentalphysik 1. Mechanik und Wärme*. Springer-Verlag, Berlin, Heidelberg, 1994.

[Dem96] W. Demtröder. *Experimentalphysik 3. Atome, Moleküle und Festkörper*. Springer-Verlag, Berlin, Heidelberg, 1996.

[DPG] DPG. Part of exposition on occasion of the central annual conference of the DPG, Physikalisch-Technische Bundesanstalt, Hermann-von-Helmholtz-Bau, Institute Berlin, 2005-03-06. http://www.ptb.de/cms/fileadmin/internet/publikationen/jahresberichte/Jahresbericht_2005/NachrichtenDesJahres/ndjs23.jpg. Accessed: 2014-07-19.

[Dzy10] O. Dzyapko. *Magnon kinetics in quasi-equilibrium under parametric pumping leading to Bose-Einstein condensation*. Doctor's thesis, Westfälische Wilhelms-Universität Münster, 2010.

[EdH15] A. Einstein and J. W. de Haas. Experimenteller Nachweis der Ampèreschen Molekularströme. *Naturwissenschaften*, 3(19):237–238, 1915.

[Fey82] R. P. Feynman. Simulating physics with computers. *International Journal of Theoretical Physics*, 21:467–488, 1982.

[GM96] A. G. Gurevich and G. A. Melkov. *Magnetization Oscillations and Waves*. CRC Press, Boca Raton, New York, London, 1996.

[HK51] C. Herring and C. Kittel. On the Theory of Spin Waves in Ferromagnetic Media. *Phys. Rev.*, 81:869–880, Mar 1951.

[HP40] T. Holstein and H. Primakoff. Field Dependence of the Intrinsic Domain Magnetization of a Ferromagnet. *Phys. Rev.*, 58:1098–1113, Dec 1940.

[HRW03] D. Halliday, R. Resnick, and J. Walker. *Physik*. Wiley-VCH Verlag GmbH, Weinheim, 2003.

[Kal80] B.A Kalinikos. Excitation of propagating spin waves in ferromagnetic films. *Microwaves, Optics and Antennas, IEE Proceedings H*, 127(1):4, February 1980.

[KDD+11] H. Kurebayashi, O. Dzyapko, V. E. Demidov, D. Fang, A. J. Ferguson, and S. O. Demokritov. Controlled enhancement of spin-current emission by three-magnon splitting. *Nature Materials*, 10(9):660–664, 2011.

[Kit48] C. Kittel. On the Theory of Ferromagnetic Resonance Absorption. *Phys. Rev.*, 73:155–161, Jan 1948.

[Kit53] C. Kittel. *Einführung in die Festkörperphysik*. Oldenbourg Wissenschaftsverlag GmbH, München, 1953.

[KPS97] M. I. Kaganov, N.B. Pustyl'nik, and T. I. Shalaeva. Magnons, magnetic polaritons, magnetostatic waves. *Physics-Uspekhi*, 40(2):181, 1997.

[KS86] B. A. Kalinikos and A. N. Slavin. Theory of dipole-exchange spin wave spectrum for ferromagnetic films with mixed exchange boundary conditions. *Journal of Physics C: Solid State Physics*, 1986.

[LP92] E. M. Lifshitz and L. P. Pitajewski. *Lehrbuch der theoretischen Physik IX: Statistische Physik Teil 2*. Akademie Verlag GmbH Berlin, 1992.

[Maj07] N. Majlis. *The Quantum Theory of Magnetism*. World Scientific Publishing, 2007.

[Nat] National Institute of Standards and Technology (NIST) in U.S. Commerce Department. Oommf. http://math.nist.gov/oommf/, Date created: 2006-08-28, Last updated: 2014-03-12. Accessed: 2014-08-12.

[NB14] P. Nowik-Boltyk. *Coherence and pertubed dynamics in magnon Bose Einstein condensates*. Doctor's thesis, Westfälische Wilhelms-Universität Münster, 2014.

[NM07] A. H. Nayfeh and D. T. Mook. *Parametrically Excited Systems*. Wiley-VCH Verlag GmbH, 2007.

[Sat11] K. D. Sattler. *Handbook of Nanophysics: Funktional Nanomaterials*. CRC Press, 2011.

[Sch] M. Schuster. Instructions to Laboratory Course about the Einstein de Haas Effect. M. Schuster, 2005, http://www.physik.kit.edu/Studium/F-Praktika/Downloads/Einstein_de_Haas_Juli08.pdf. Accessed: 2014-05-19.

[Suh57] H. Suhl. The theory of ferromagnetic resonance at high signal powers. *Journal of Physics and Chemistry of Solids*, 1(4):209 – 227, 1957.

[Ulr] H. Ulrichs. Spin Wave App. http://www.uni-muenster.de/Physik.AP/demokritovdaten/spinwaveapp.html. Accessed: 2014-08-22.

[Ulr14] H. Ulrichs. *Spin-wave instabilities on the nanoscale*. Doctor's thesis, Westfälische Wilhelms-Universität Münster, 2014.

[Van] A. Vansteenkiste. DyNaMat group, Ghent University, Belgium. Mumax. http://mumax.github.io/. Accessed: 2014-08-12.

[VVdW] A. Vansteenkiste and B. Van de Wiele. MuMax: a new high-performance micromagnetic simulation tool. arXiv:1102.3069. 2011.

[WAB+01] S. A. Wolf, D. D. Awschalom, R. A. Buhrman, J. M. Daughton, S. von Molnár, M. L. Roukes, A. Y. Chtchelkanova, and D. M. Treger. Spintronics: A spin-based electronics vision for the future. *Science*, 294(5546):1488–1495, 2001.